

Contractor Report ARLCD-CR-83053

**TECHNICAL
LIBRARY**

SUPERCONDUCTIVITY FOR ELECTROMAGNETIC GUNS

Osman K. Mawardi
Collaborative Planners, Inc.
15 Mornington Lane
Cleveland Heights, Ohio 44106

March 1984



U.S. ARMY ARMAMENT RESEARCH AND DEVELOPMENT CENTER

LARGE CALIBER WEAPON SYSTEMS LABORATORY

DOVER, NEW JERSEY

Approved for public release, distribution unlimited.

The views, opinions, and/or findings contained in this report are those of the author(s) and should not be construed as an official Department of the Army position, policy, or decision, unless so designated by other documentation.

The citation in this report of the names of commercial firms or commercially available products or services does not constitute official endorsement by or approval of the U.S. Government.

Destroy this report when no longer needed Do not return to the originator.

UNCLASSIFIED

SECURITY CLASSIFICATION OF THIS PAGE (When Date Entered)

REPORT DOCUMENTATION PAGE		READ INSTRUCTIONS BEFORE COMPLETING FORM
1. REPORT NUMBER Contractor Report ARLCD-CR-83053	2. GOVT ACCESSION NO.	3. RECIPIENT'S CATALOG NUMBER
4. TITLE (and Subtitle) SUPERCONDUCTIVITY FOR ELECTROMAGNETIC GUNS		5. TYPE OF REPORT & PERIOD COVERED Final Technical Report Period 9/17/82 to 9/17/83
		6. PERFORMING ORG. REPORT NUMBER
7. AUTHOR(s) Osman K. Mawardi		8. CONTRACT OR GRANT NUMBER(s) DAAK-10-82-C-0245
9. PERFORMING ORGANIZATION NAME AND ADDRESS Collaborative Planners, Inc. 15 Mornington Lane Cleveland Heights, Ohio 44106		10. PROGRAM ELEMENT, PROJECT, TASK AREA & WORK UNIT NUMBERS
11. CONTROLLING OFFICE NAME AND ADDRESS ARDC, TSD STINFO DIV [DRSMC-TSS(D)] Dover, NJ 07801		12. REPORT DATE March 1984
		13. NUMBER OF PAGES
14. MONITORING AGENCY NAME & ADDRESS (if different from Controlling Office) ARDC, LCWSL Applied Sciences Div [DRSMC-LCA-G]		15. SECURITY CLASS. (of this report) Unclassified
		15a. DECLASSIFICATION/DOWNGRADING SCHEDULE
16. DISTRIBUTION STATEMENT (of this Report) Approved for public release, distribution unlimited.		
17. DISTRIBUTION STATEMENT (of the abstract entered in Block 20, if different from Report)		
18. SUPPLEMENTARY NOTES		
19. KEY WORDS (Continue on reverse side if necessary and identify by block number) SYNCHRONOUS ACCELERATORS SWITCHLESS COAXIAL ACCELERATOR		
20. ABSTRACT (Continue on reverse side if necessary and identify by block number) This report deals with a feasibility study for an electromagnetic gun using superconducting components. The report discusses two questions. The first deals with an assessment of the applied superconductivity technology, while the second is concerned with two reference designs for coaxial accelerators making use of advanced energy transfer concepts. Impressive recent developments in the technology of cryogenic insulation and of liquid helium liquifiers, as well as, of commercially available super-		

DD FORM 1 JAN 73 1473

Unclassified

SECURITY CLASSIFICATION OF THIS PAGE (When Date Entered)

conductors makes it possible to construct superconducting pulsed power sources of very high efficiency and of remarkable compactness and low weight. Repetitive superconducting switches, together with superconducting storage inductors makes these pulsed sources very competitive with conventional sources in terms of reliability and time constant.

The synchronous coaxial accelerators investigated in this report rely on a simple procedure that eliminates the need for switches. It is based on the concept of transferring the energy of the pulsed source to a transmission line. The driver coils are part of the transmission line. Consequently, as the pulse travels down the line, the coils are excited in sequence and in synchronism with the moving driven coil. Since the energy is transferred from the pulsed source to a transmission line which appears as a resistive load, the transfer efficiency is very high.

Other features of the novel designs consist in maintaining the current in the driven coil to a very low value thus minimizing the problem of arcing at the brushes and in dealing with the high voltage required to drive the guns.

TABLE OF CONTENTS

Assessment of Technology	1
Superconductors	1
Introduction	1
High Current Density (Type II) Superconductors	3
Superconductivity in Hydrides	6
Stabilization of Superconductors	7
Critical Current	10
Internally Cooled Cabled Superconductors (ICCS)	12
Cryogenics for System	15
Superinsulators	15
Size & Power Requirements of 4.2°K Refrigerators	18
Introduction	18
Thermal Efficiency	18
Input Power Requirements	19
Refrigerator Weight	20
Refrigerator Volume	23
Pulsed Sources	23
Introduction	23
Energy Transfer Systems	28
Introduction	28
Energy Transfer Mechanisms	31
Reference Designs	33
General Remarks	33
Temporal Character of Source	33
Outline of Design I	37
Interior Ballistics of Gun	39
Propagation of Transient on Transmission Line	43
Characteristics of Pulsed Source	44
Storage Coil	48
Conductors Characteristics	49
Coil Structure	56

Table of Contents, Con't

Mass of Storage Coil	57
Flux Pump	58
Driver Coils	62
Design of Driven Coil	65
Cooling Load	65
Heat Losses from Switch	67
Heat Losses from Storage Coil	67
Heat Losses from Pump	67
Capacity of Cooling Plant	68
Summary and Conclusions for Reference I Design	68
Outline of Reference Design II (RD II)	70
Basic Concept	70
Construction Features of Gun	72
Conclusions	72
References	79
Appendices	
A. Design Details for Reference Design II	
B. Computer Algorithm for Solution of the Coaxial Accelerator	

List of Figures

- Figure 1. Profiles of current density and flux density through one vortex of the triangular flux array of a type II superconductor.
- Figure 2. Upper critical fields of V-based A15 compounds.
- Figure 3. Upper critical fields of Nb-based A15 compounds and Mo_3Os .
- Figure 4. Comparison of the critical current density of NbTi and two commercial forms of Nb_3Sn .
- Figure 5. Magnetic field dependence of overall J_c (Core+Bronze+Barrier) of multi-filamentary Nb_3Sn conductors with improved high-field performances.
- Figure 6. Temperature dependence of the critical current in NbTi and Nb_3Sn .
- Figure 7A. Hollow conductor developed by Morpurgo.
- Figure 7B. Internally cooled cable developed by MIT.
- Figure 8. Effective thermal conductivity of a multi-layer insulation. Of alternate layers of fiberglass and aluminum foil.
- Figure 9. Dependence of the thermal conductivity on the gas pressure. The curves shown are for a 60/layers/in multilayer insulator kept between 90° and 300°K .
- Figure 10. Dependence of an insulator thermal conductivity on the temperature. The curve refers to the case of crinkled aluminized polyester multi-layers insulators.
- Figure 11. Specific power requirement for liquid helium refrigerators.
- Figure 12. Specific weight as a function of capacity.
- Figure 13. Specific size of refrigerators as a function of their capacity.
- Figure 14. Circuit for transfer from separate inductors.
- Figure 15. Dependence of the inductance and resistance on the time constant of the coil.
- Figure 16. Transfer from transformer coupled inductors.
- Figure 17. Cost of energy storage vs. current rise time.
- Figure 18. Cost of energy storage vs. current rise time for pulsed system.

List of figures, con't

- Figure 19. Weight per unit energy of some coils as a function of E.
- Figure 20. Possible transfer circuits for energy cycling between inductive storage and load systems.
- Figure 21. Block diagram for synchronous accelerator.
- Figure 22. Geometry of driver and driven coils.
- Figure 23. Functional dependence of $v(t)$.
- Figure 24. Forces appearing on coil over one full traverse.
- Figure 25. Dependence of the Velocity on the position of the projectile.
- Figure 26. Typical circuit used in the transmission line lattice.
- Figure 27. Evolution of pulse down the gun.
- Figure 28. Dimensions of trooidal storage coil.
- Figure 29. Dependence of the magnetic field on the size of the torus and on the energy stored.
- Figure 30. Dependence of the energy stored on the maximum field used.
- Figure 31. Dependence of the energy on the inductance of the storage coil.
- Figure 32. Nomograph for the coil parameters.
- Figure 33. 503 strand lattice braid conductor.
- Figure 34. Construction details for the winding support.
- Figure 35. Cross section through storage coil.
- Figure 36. Configuration of flux pump magnets.
- Figure 37. Method of compounding three flux pumps.
- Figure 38. Temporal variation of the rotating magnetic field to actuate the flux pump.
- Figure 39. Coil dimensions.
- Figure 40. Location of the coils for equal intervals for the transmit time of the projectile.

List of figures, Con't

Figure 41. Schematic of gun used in RD II.

Figure 42. E M gun.

Figure 43. Pulsed source.

Figure 44. Transformer.

List of Tables

- Table 1. Superconducting transition temperature T_c (K) of binary Al5 phases.
- Table 2. Physical properties.
- Table 3. Comparison of NbTi S/C in two arrangements - (ICCS & hollow conductors).
- Table 4. Summary of some typical sizes.
- Table 5. Comparison of cooling power requirements.
- Table 6. Design parameters of available refrigerators.
- Table 7. Design criteria for guns.
- Table 8. Inductance needed for various pulses.
- Table 9. Charging times for various gun ratings.
- Table 10. Source characteristics needed for various inductors.
- Table 11. Summary of data.
- Table 12. Conductor characteristics.

ASSESSMENT OF TECHNOLOGY

Superconductors

Introduction

The ability of superconductors to maintain zero electrical resistance under direct current conditions while in the presence of high magnetic fields has led to various current and future proposed uses of superconducting coils. The subject matter of this report deals with coils which will be expected to operate under pulsed conditions and which will produce intense mechanical forces. The heart of the system is the superconducting wire which will carry the current required to generate the magnetic field and which will be able to sustain the superconducting state under these extreme conditions.

The material covered, therefore, will discuss the superconductors presently available, the chief parameters describing the characteristics of the superconductors and the usual procedure used in cooling the conductors.

As it is well-known, there are two types of superconducting material (ref 1) soft (or Type I) superconductors and hard (or Type II) superconductors. The critical magnetic field of Type I superconductors is quite low (a few hundred Acm^{-1}). These materials are of interest to large current low magnetic field applications such as switches.

Type II superconductors by contrast to soft superconductors remain superconducting in high fields. For this reason, Type II superconductors are essential to the construction of magnets or other applications requiring high fields.

Hard superconductors exhibit an incomplete Meissner effect (ref 2). They have the tendency to form a structure of mixed normal and superconducting regions. This mixed state structure is necessary to explain the penetration of the flux

in Type II material. On the basis of theoretical work (ref 3) which has been verified experimentally, (ref 4) it appears that the normal regions consist of cores whose radius is of the order of the coherent length of the superconducting electrons. Flux is trapped in these cores. Surrounding these cores (fig. 1) there are superconducting matrices in which the magnetic field penetrates with a characteristic length of λ (the London thickness).

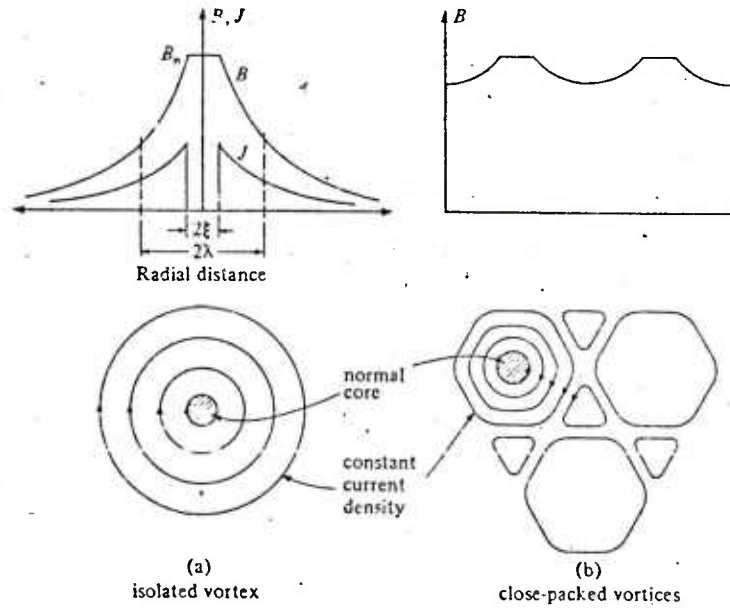


Figure 1. Profiles of current density and flux density through one vortex of the triangular flux array of a type II semiconductor.

One would have thought that Type II superconductors having a high critical field would also have a high current density-carrying capacity commensurate with these high fields. In fact, this is not the case. It is well-known to workers in applied superconductivity (ref 5) that the appearance of the mixed state plays major role in limiting the current capacity. When a transport current flows in the superconductor, there is a dissipation of energy, which is caused by the com-

bined flow of the trapped flux in the normal regions and by the diffusion of the external flux into the conductor (as observed by the incomplete Meissner effect).

Now, this dissipation of energy causes a rise in temperature of the normal region, leading to further flow. This phenomenon can become a regenerative process that may cause the current carrying conductor to quench. The manner in which this runaway process is prevented is discussed in a subsequent section on the conductors stabilization.

High Current Density (Type II) Superconductors

The highest known superconducting transition temperature has always remained within the class of A-15 type material (ref 6). The designation of the A-15 type structure started in 1931 when Hartmann (ref 7) reported a new modification of Tungsten (β -W). Later conclusions, attributing the β -form to a suboxide W_3O , proved to be inexact. Whether or not some oxygen contamination is necessary to actually stabilize β -W cannot be decided with certainty. An A-15 type modification has also been found for chromium fine particles. The parent compound Cr_3Si is now more widely used to designate the structure type.

The real story of the A-15 compounds began with the discovery of high superconducting transition temperatures for V_3Si and Nb_3Sn by Hardy and Hulm (ref 8) and Matthias (ref 9).

Table 1 given below presents a summary of the transition temperatures found for various compounds.

Table 1. Superconducting transition temperatures (T_c (K) of binary Al5 phases (ref 6)

Compound	Transition($^{\circ}$ K)	Compound	Transition($^{\circ}$ K)
Ti_3Sb	6.5	Ti_3Ir	4.2
$Zr_{80}Sn_{20}$	0.92	Ti_3Pt	0.5
Zr-Pb	0.76	Zr_3Au	0.9
$Zr_{\sim 3}Bi$	3.4		
V-Al	11.8	$V_{29}Re_{71}$	8.4
V_3Ga	15.9	$V_{50}Os_{50}$	5.7
V_3Si	17.0	$V_{65}Rh_{35}$	≈ 1
$V_{\sim 3}Ge$	6-7.5	$V_{63}Ir_{37}$	1.7
$V_{\sim 3}Ge$	6-11	$V_{\sim 3}Pd$	0.08
$V_{\sim 79}Sn_{\sim 21}$	4.3	V_3Pt	3.7
V-Sn	7-17	$V_{76}Au_{24}$	3
$V_{77}As_{23}$	0.2		
$V_{76}Sb_{24}$	0.8	$Nb_{75}Os_{25}$	1.0
Nb_3Al	19.1	$Nb_{75}Rh_{25}$	2.6
Nb_3Ga	20.7	$Nb_{72}Ir_{28}$	3.2
$Nb_{\sim 3}In$	8.9-2	Nb_3Pt	11
$Nb_{82}Si_{18}$	4.4	$Nb_{\sim 3}Au$	11.5
Nb-Si	9.3		
Nb-Si	4.8	$Cr_{72}Ru_{28}$	3.4
Nb-Si	11-17	$Cr_{73}Os_{27}$	4.7
Nb-Ge	6-17	$Cr_{78}Rh_{22}$	0.07
Nb-Ge	23	$Cr_{82}Ir_{18}$	0.75
Nb_3Sn	18		
Nb-Sb	2	$Mo_{40}Tc_{60}$	13.4
$Nb_{\sim 3}Bi$	3	$Mo_{\sim 65}Re_{\sim 35}$	≈ 15 (A15)
		$Mo_{75}Os_{25}$	12.7
$Ta_{\sim 3}Ge$	8	$Mo_{78}Ir_{22}$	8.5
$Ta_{\sim 3}Sn$	8.3	$Mo_{82}Pt_{18}$	4.6
$Ta_{\sim 3}Sb$	0.7		
		$W_{\sim 60}Re_{\sim 40}$	11
Mo_3Al	0.58		
Mo_3Ga	0.76		
$Mo_{77}Si_{23}$			
$Mo_{77}Ge_{23}$			

The figures 2 and 3 below (ref 10) below show the dependence of the critical field on the temperature for the V-based and Nb based A-15 compounds.

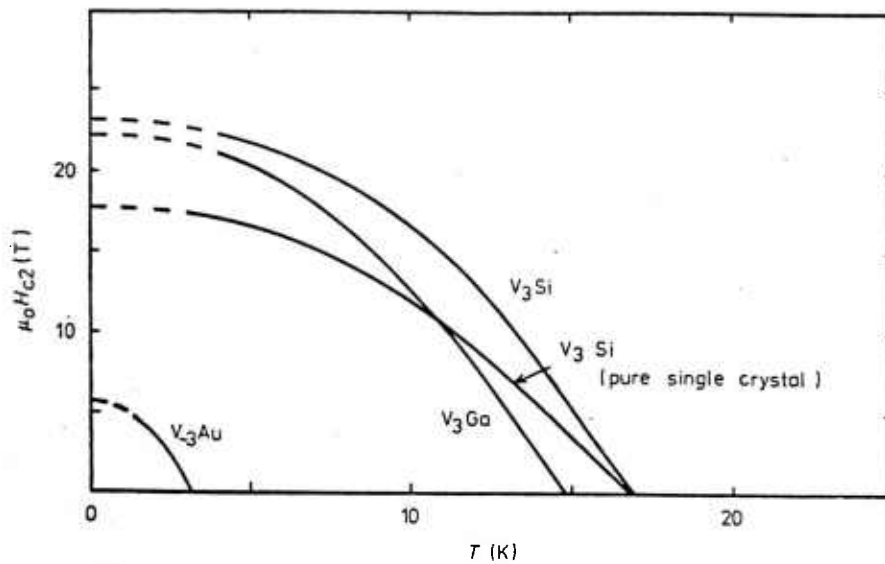


Figure 2. Upper critical fields of V-based A15 compounds

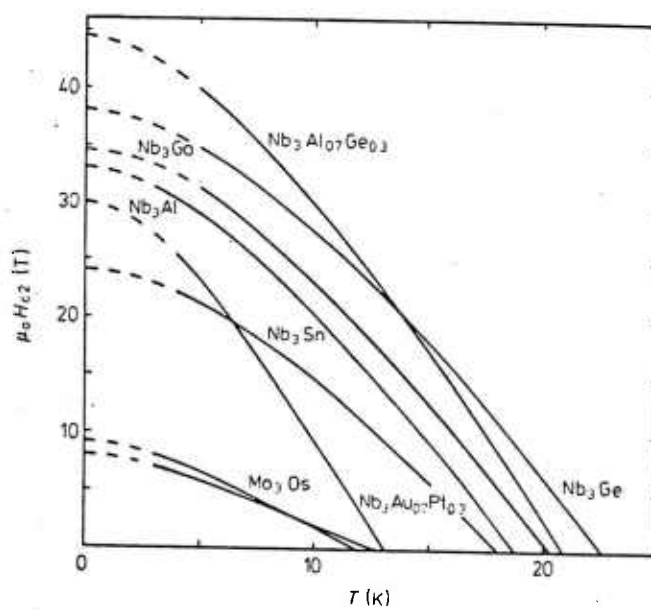


Figure 3. Upper critical fields of Nb-based A15 compounds and Mo_3Os .

The conductors can be constructed either in the form of filaments or tapes. The Nb_3Sn tape made by the surface diffusion process is widely used for the construction of 15-T class superconducting magnets. The V_3Ga tape made by the surface diffusion process has been used for the construction of the 17.5T superconducting magnet, which established the highest field record in the superconducting state.

The invention of the composite process (ref 11) made it possible to fabricate the multifilamentary type Al5 wires that are much more stable than the surface diffusion process tapes in time varying fields. Recently, the in-situ technique (ref 12) for the fabrication of filamentary composites has become of great interest since it is a superior alternative to the composite process. This new process consists of casting a two-phase material and subsequent cold working and heat treatment, thus producing an array of aligned and discrete superconducting filaments in a ductile matrix.

There is a great deal of experimental evidence to show that in-situ formed Nb_3Sn superconductors have a critical current comparable to that of conventional conductors with the advantage of superior mechanical property.

Superconductivity in Hydrides

In view of the recent interest shown (ref 13) in the H-charged systems, a short section has been devoted to the review of these interesting compounds. The Pd-H system has been studied extensively in particular after Skoskiewicz reported the occurrence of superconductivity in this compound. Since then, it was found that superconductivity takes place for Pd-D and Pd-M-H(D) where M is one of the noble metals Cu, Ag or Au. The highest transition temperature observed was 16.6K for an alloy with $\text{H/Pd}_{55}\text{Cu}_{45} \approx 0.7$.

The superconducting properties (ref 14) of hydrogen doped Nb_3Sn are very sensitive to the hydrogen content x in Nb_3SnH_x . Between a field of 9T to 12T the critical temperature shows a slight maximum at $x \approx 0.02$ after which it decays abruptly. Also, the critical current density is somewhat higher than the unhydrogenated samples with the enhancement being highest at 6K.

The high H concentration required in these alloys in order to obtain superconductivity has been achieved in one of several ways: electrolytic charging at room and dry-ice temperature, high-pressure charging at several bars, precharging at 4 bar and 300°C with subsequent implantation of H at liquid He temperature and codeposition of H and Pd at 4K.

Interesting as these compounds are, there does not appear to be a substantial enhancement of the superconducting properties to warrant the added manufacturing cost.

Stabilization of Superconductors (ref 15)

In addition to being mechanically sound, conductors must operate reliably in the magnet windings. To provide stability against disturbances of electrical, thermal or mechanical nature which may occur in the windings, a material of high electrical and thermal conductivity is included in the conductor. Copper is used primarily in the alloy system. Silver and copper have been used to stabilize Nb_2Sn conductors. Although it has a higher electrical conductivity than copper (especially at high magnetic fields), high purity aluminum has found limited use as an integral part of the conductor because of the problem of making a metallurgical bond with the superconductor. In some instances, a combination of aluminum and copper have been used where the copper acts as an intermediate between the aluminum and the superconductor.

The question of stability of a superconductor is best understood by referring to table 2 which summarizes some thermal and magnetic properties for three superconductors normally used. Inspection of table 2 indicates that magnetic field changes in a superconductor take place more rapidly than heat can be conducted away by thermal diffusion. On the other hand, for copper or aluminum thermal diffusion takes place much faster than magnetic field changes. For this reason, the last two metals are effective stabilizing substrates. Furthermore, the high specific heat of helium makes it a useful sink.

The criterion for stability is found by equating the heat generated by the conductor to the heat transferred from the conductor to the liquid Helium. One this obtains the stability requirements to be:

1. the temperature in the conductor with all the current flowing in the substrate must be less than the critical temperature of the superconductor. This specific condition thus becomes a question of heat transfer design in which the conductors size (and small passages between the coil turns) are optimized for a heat transfer to helium of the order of 0.8 w/cm^2 and will all the current in the substrate.
2. The size of the superconductors should be less than a certain size in order that the temperature drop in them be small.

For steady state conditions, computed values for Nb-Ti and copper composites, indicate that the strand sizes should be of the order of 50-100 microns. For a.c. conditions and because of eddy current losses in the substrate, the superconducting filaments are given a helical twist in accordance with standard high frequency procedures to minimize losses in conductors. More accurate calculations for these conditions yield strand sizes for the same material of about 6 microns

Table 2. Physical properties

	Nb ₃ Sn	Nb-Zr	Nb-Ti	Copper	Aluminum	Liquid	Helium Gas
Thermal conductivity (mW/cm K)	$\frac{0.4}{\kappa}$	$\frac{0.8}{\kappa}$	$\frac{1.2}{\kappa}$	$\frac{7000}{\kappa}$	$\frac{3335}{\kappa}$	$\frac{2.72}{\kappa}$	$\frac{0.1}{\kappa}$
Specific heat (mJ/g K)	0.21	0.18	0.18	0.099	0.0077	4480	6000
Normal resistivity 4.2K (ohm cm)	26	34	24	0.03	--	--	--
Specific gravity (gm/cm ³)	5.4	8.1	5.6	8.9	2.7	0.125	0.008
Critical temperature (K)	18	10.5	9.5	--	--	--	--
Thermal diffusivity (cm ² /sec)	$\frac{0.35}{\kappa_c}$	$\frac{5.4}{\kappa_c}$	$\frac{1.18}{\kappa_c}$	$\frac{7900}{\kappa_c}$	$\frac{--}{\kappa_c}$	$\frac{0.005}{\kappa_c}$	$\frac{0.002}{\kappa_c}$
Electrical diffusivity (cm ³ /sec)	2069	2706	1910	2.5	--	--	--
Ratio of diffusivities	$\frac{0.00169}{\gamma_{cp}}$	$\frac{0.020}{\gamma_{cp}}$	$\frac{0.0062}{\gamma_{cp}}$	$\frac{7600}{\gamma_{cp}}$	--	--	--

Critical Current

Critical current is considered to be the primary parameter for most applications of superconductors. The critical current will determine the amount of material required for a coil design.

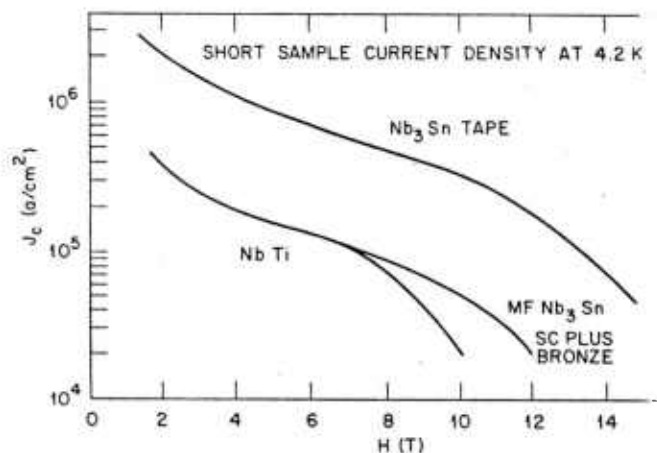


Figure 4. Comparison of the critical current density of NbTi and two commercial forms of Nb₃Sn.

Figure 4 shows the dependence of the critical current density on the field for two forms of Nb₃Sn and Nb-Ti (ref 16). These measurements show that the Nb₃Sn tape enjoys a clear superiority in current density. In multifilamentary form the early measurements on Nb₃Sn did not show an advantage over Nb Ti up to 7T.

The recent in-situ process for the construction of multifilamentary Nb₃Sn shows an impressive improved performance specially at very high fields (> 7T). Figure 5 shows typical measurements fabricated by various Japanese firms (ref 17).

The dependence of the critical current density on the temperature is shown in a more graphic manner in figure 6 (ref 18). Here again, the superiority of Nb₃Sn at high fields is evident.

Several designs for superconducting coils in the 8 to 10 Teslas have been completed and reported in the literature (ref 19).

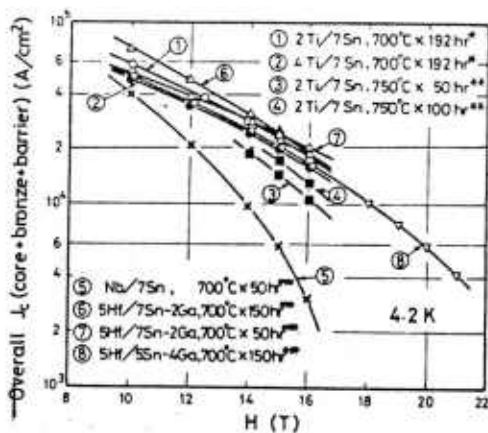


Figure 5. Magnetic field dependence of overall J_c (Core+bronze+barrier) of multifilamentary Nb_3Sn conductors with improved high-field performances.

- * 160-core wire; bronze ratio: 3.0; fabricated by NRIM.
- ** 2440-core tape; bronze ratio: 1.7; by Furukawa.
- *** 331-core wire; bronze ratio: 2.5; by Hitachi.

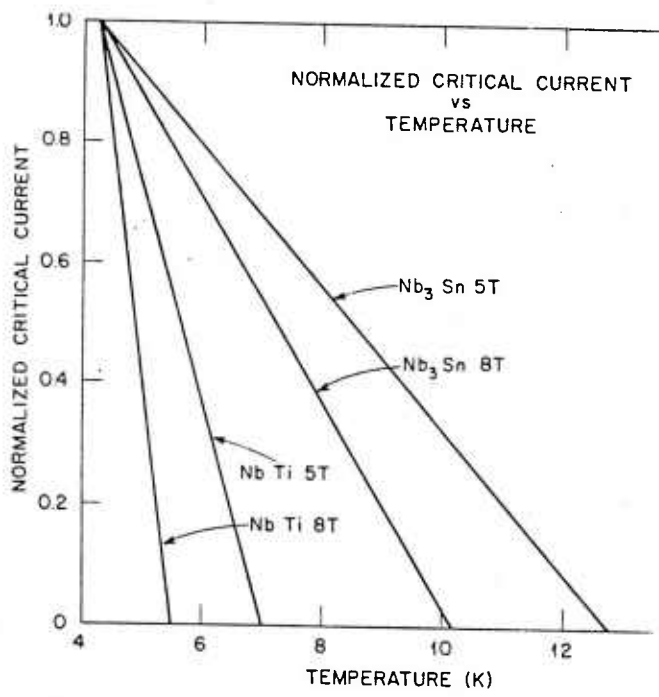


Figure 6. Temperature dependence of the critical current in $NbTi$ and Nb_3Sn .

Internally Cooled Cabled Superconductors (ICCS)

Internally cooled cabled superconductors have been incorporated into a number of installations both in the U.S. and overseas. The basis of operation (ref 20) of the ICCS consists in placing a multistrand cable, containing a superconductor and its stabilizer in a conduit in which superfluid helium is forced to circulate.

The ICCS is a high surface area superconductor in which superconducting strands interface with the coolant. There is a dramatic increase in the heat transfer surface as a result of this method of construction. Table 3 (ref 21) summarizes the characteristics of two conductors: one is an ICCS and the other is a hollow conductor (fig. 7). The conductors are assumed to carry 16,000A, are of NbTi and are operating at 8T.

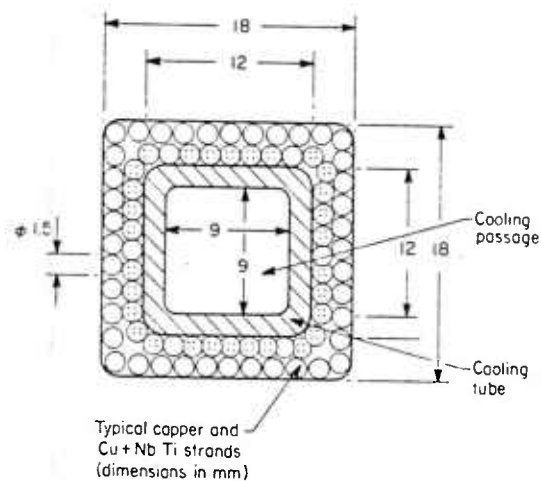


Figure 7A. Hollow conductor developed by Morpurgo (ref 21).

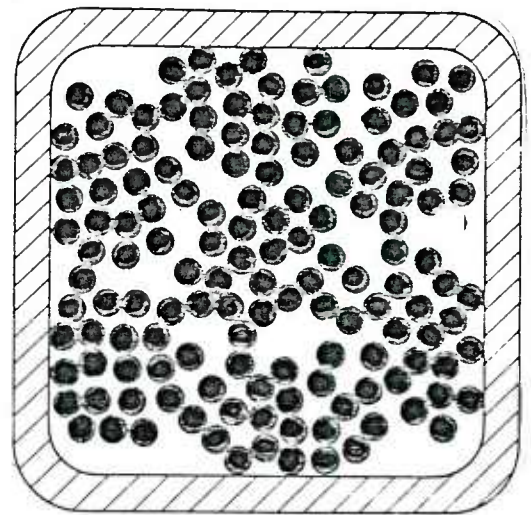


Figure 7B. Internally cooled cable developed by MIT (ref 21).

Table 3. Comparison of NbTi S/C in two arrangements - (ICCS and hollow conductors)

	Cabled 972 strands	Hollow conductor
Cross sectiona area of copper m/m^2	143.7	219.5
Copper: supercond. ratio	4:1	4:1
Cu (fraction)	0.8	0.8
J, A/mm^2 in copper	139.2	91.1
Heating rate (W/cm^2)	15.5	6.6
Heat transfer surface (cm^2/cm)	149.6	4.3
Cooling flux required (W/cm^2)	0.1	1.53
h at $\Delta T = 1.4^\circ\text{K}$	0.07	1.10
Hydraulic diam cm	0.038	1.36
Nu number	13	6,800
Re number	4,000	9×10^6
Flow rate/unit area ($\text{g/cm}^2\text{s}$)	4	245
Velocity (cm/sec)	30	1,800
Pressure drop	1.1	25

Because of the superior properties of Nb_3Sn over NbTi, series of tests (ref 22) were carried at the MIT National Magnet Laboratory on behalf of DOE to investigate the feasibility of ICCS cables constructed with Nb_3Sn conductors.

The main conclusions arrived at as a result of this study are that:

1. Nb_3Sn appears to be less brittle than originally considered and lends itself well to the ICCA concept.
2. The ICCS sheath serves many purposes. It is a hydraulic conduit which must be leak tight at liquid helium temperatures and operating pressures

of 3 to 15 atmos. It is also a high pressure conduit during quench which must sustain pressures of the order of 200 atmos. The sheath is also a major tensile and compression member, protecting the cable from magnetic pressure.

3. The ICCS helium charge facilitates removal of heat from the cable irrespective of bulk flow. The interstitial helium also acts as a secondary coolant for the removal of accumulated heat. A modest bulk flow is required provided that the interstitial helium is supercritical. Subcritical or boiling two phase helium, facilitates equally primary heat transfer as long as its low density vapor fraction is minimal. The ICCS does not recover from even minor thermal disturbances if filled with low density vapor.
4. ICCS can operate at coil space current densities of $2 \text{ to } 3 \times 10^3 \text{ A/cm}^2$. As the inductance of the coil increases quench protection must be enhanced by increasing the copper stabilizer content of the cable.
5. The ICCS transient thermodynamics is still not too well understood. Initially, one observes a relatively high initial heat transfer rate for about 5 msec. This initial thermal diffusivity regime is followed by a higher and longer lasting internally generated heat transfer rate. There appears to be a delay between the dying initial heat transfer phase and buildup of the recovery phase. This delay is of the order of the time of propagation of the sound speed in the helium and the geometry of the ICCS rather than the size of the disturbed zone.

Cryogenics for System

Superinsulators

An estimate for the power required for the cooling plant will be obtained from an evaluation of the heat losses due to conduction, convection and radiation from the surroundings which will conspire towards heating (and hence, evaporating) the liquid helium, as well as, of the heat generated inside the pulse sources as a result of the departure of the source from a 100% efficiency operation. More precisely, the latter heat load consists of losses in the storage coil, in the superconducting switches and in the flux pump.

The superconducting source is visualized to operate without a liquid nitrogen shield. The elimination of the shield simplifies the construction of the system, however, this advantage is traded with an increase in heat losses. To minimize these losses the liquid nitrogen shield is replaced with multilayers of superinsulation that are vacuum packed (ref 23). As is well-known, superinsulation consists of alternate layers of a highly reflecting material, such as aluminum foil or aluminized mylar separated by spacers of thermal insulators such as fiberglass, paper, glass fabric or nylon. The whole composite is then enclosed in a vacuum jacket.

The effective thermal conductivity of the multilayers insulation depends on the number of layers packed per unit length. The conductivity goes through a minimum around 70 layers per inch (fig. 8). The figure shows the characteristics for superinsulators consisting of alternate layers of fiber glass and aluminum foil maintained between 77 and 300°K. The minimum referred to above reflects a trade-off between losses by conduction and radiation.

Convection losses on the other hand, are very pressure sensitive. As the entrapped air (between the layers of superinsulation) goes from a particle-particle

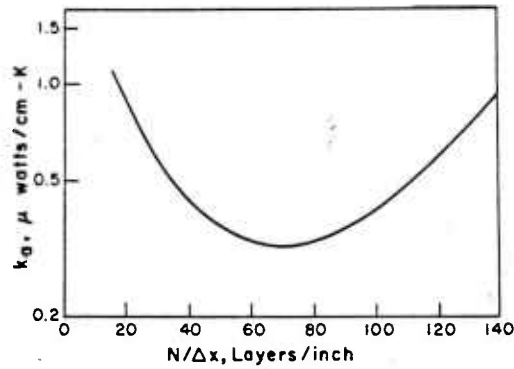


Figure 8. Effective thermal conductivity of a multi-layer insulation. Of alternate layers of fiberglass and aluminum foil. (ref 23)

collision dominated regime to the so-called Knudsen flow (ref 24), the conductivity changes appreciably as shown in figure 9.

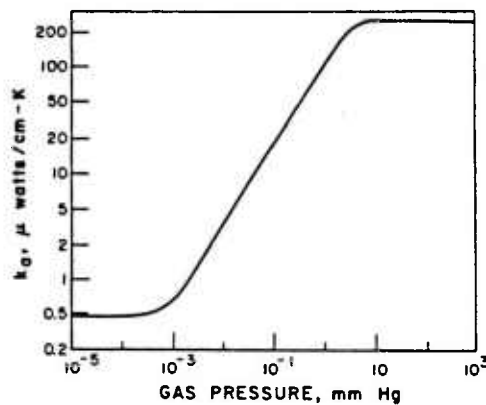


Figure 9. Dependence of the thermal conductivity on the gas pressure. The curves shown are for a 60/layers/in multilayer insulator kept between 90 and 300°K (ref 24)

The coefficient of thermal conductivity of an insulator is also a sensitive function of the temperature. The coefficient remains constant below 20°K and increases fairly rapidly above 100°K.

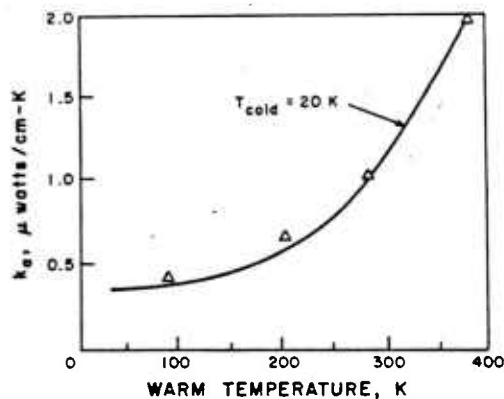


Figure 10. Dependence of an insulator thermal conductivity on the temperature. The curve refers to the case of crinkled aluminized polyester multilayers insulators.

The results of the above figure (ref 25) indicate that there is a distinct advantage in reducing the temperature of the surroundings of the system by such procedures as a liquid nitrogen shield or by vapor cooling by means of the escaping He.

A final comment refers to the edge effects. Most published values for the thermal coefficients are those for small samples measurements obtained with guard shields to minimize the losses through the edges. In practice, such idealized conditions are rarely encountered. As a result, the effective coefficients are greater by a factor of two from the published figures.

The reason for this degradation in the insulating capability can be ascribed to the combined influence of edge exposure of the boundaries, imperfections in the installation such as gaps, joints or penetration of the insulation blanket by sharp corners and by the fill and vent lines. All these causes conspire in producing a lateral conductivity in the insulator.

A practical value reasonably reflecting conditions observed in the field is $1 \mu\text{W}/\text{cm}^2\text{K}$ for a 60 layers per inch superinsulation evacuated to below 10^{-4} Torr. pressure.

Size and Power Requirements of 4.2°K Refrigerators

Introduction

A question of great interest to the system designer of electromagnetic guns is related to the rating (size, weight and power) of the liquid helium refrigerators. It is not intended, here, to go into the details of the thermodynamics of refrigeration, instead, we will concentrate on the rating aspects and remind the reader of the various possible thermodynamic cycles that have been used in the design of refrigerators. The four mentioned below have been used more commonly (ref 26) either singly or in combinations.

1. Cascade Joule-Thomson process
2. Claude Cycle
3. Stirling Cycle
4. Gifford - Mc Mahon cycle

The Joule-Thomson process is used in the lowest stage of almost all liquid He refrigerators.

Thermal Efficiency

A figure of merit of a refrigerator is its thermal efficiency. This number is measured with respect to the absolute or reversible (Carnot) efficiency and is found from

$$\begin{aligned} \text{Thermal efficiency (also called Percent Carnot)} \\ = 100 (W_c/Q \text{ Carnot} / (W_c/Q) \text{ actual}) \end{aligned}$$

In the above, W_c is the work of compression and Q is the net refrigeration produced. The Percent Carnot efficiency for small machines is about 1% while for

a large machine it can be as high as 15%.

Input Power Requirements

A survey of the input power needed to drive liquid He refrigerators of various designs has been compiled by Strobbridge (ref 27) et al.,.The findings of the survey is shown in graphical form in figure 11. As expected, the input power of 1kW/watt of cooling power which is often quoted worsens as the capacity falls below 10 Watts of cooling and improves to the value of 400 Watts/Watt for machines providing a few kilowatts of cooling.

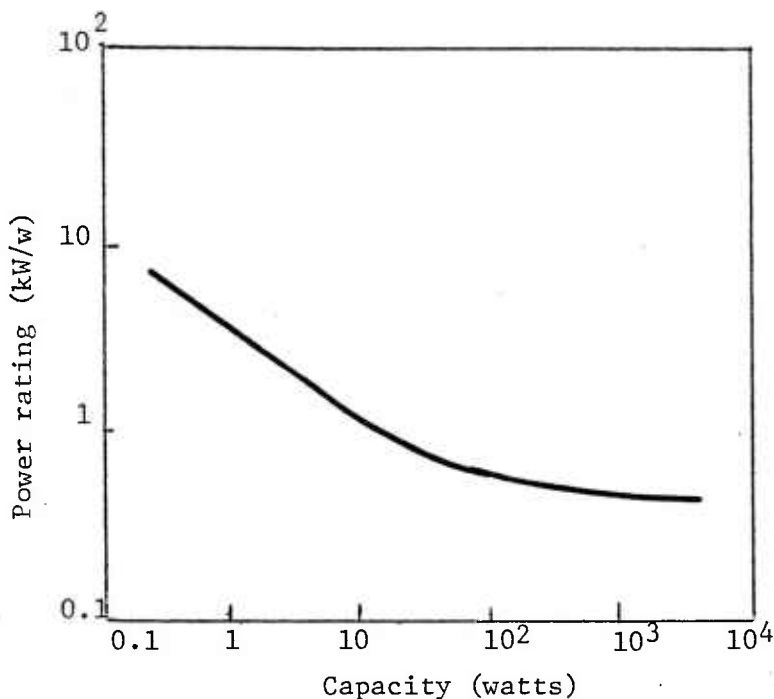


Figure 11. Specific power requirement for liquid helium refrigerators.

Refrigerator Weight

Very little effort has been expended so far in keeping down the weight of the refrigerator. Past practice mainly used available equipment and the required cooling power is achieved by cascading the optimum combination of refrigerating stages.

Even so, there is an impressive reduction in the weight per unit by cooling capacity as the capacity is increased.

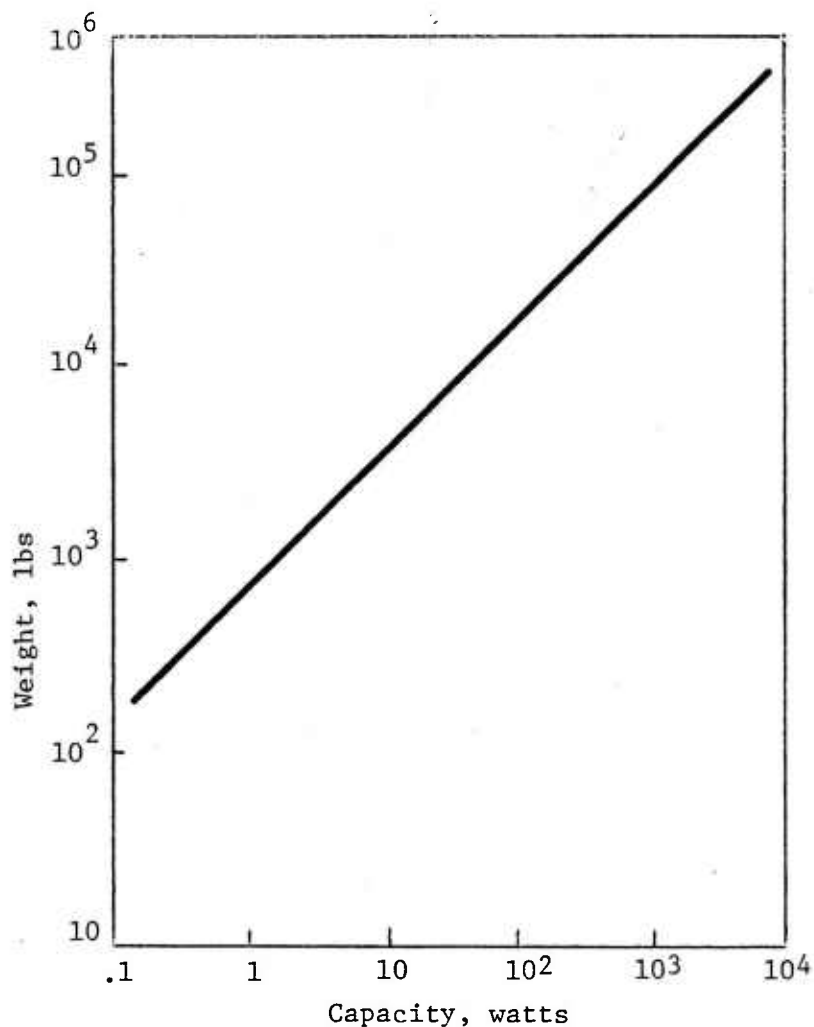


Figure 12. Specify weight as a function of capacity

Discussion with several manufacturers led us to conclude that this specific weight can indeed be improved upon if there was an incentive in the form of a specific market demand.

Refrigerator Volume

Another parameter of great interest to the designer of Electromagnetic gun systems is the volume (size) of the liquid Helium refrigerators, Strobbridge et al., (ref 27)

included the data they found in their survey. Their data are summarized in figure 13 and table 4 below which gives a summary of some typical sizes.

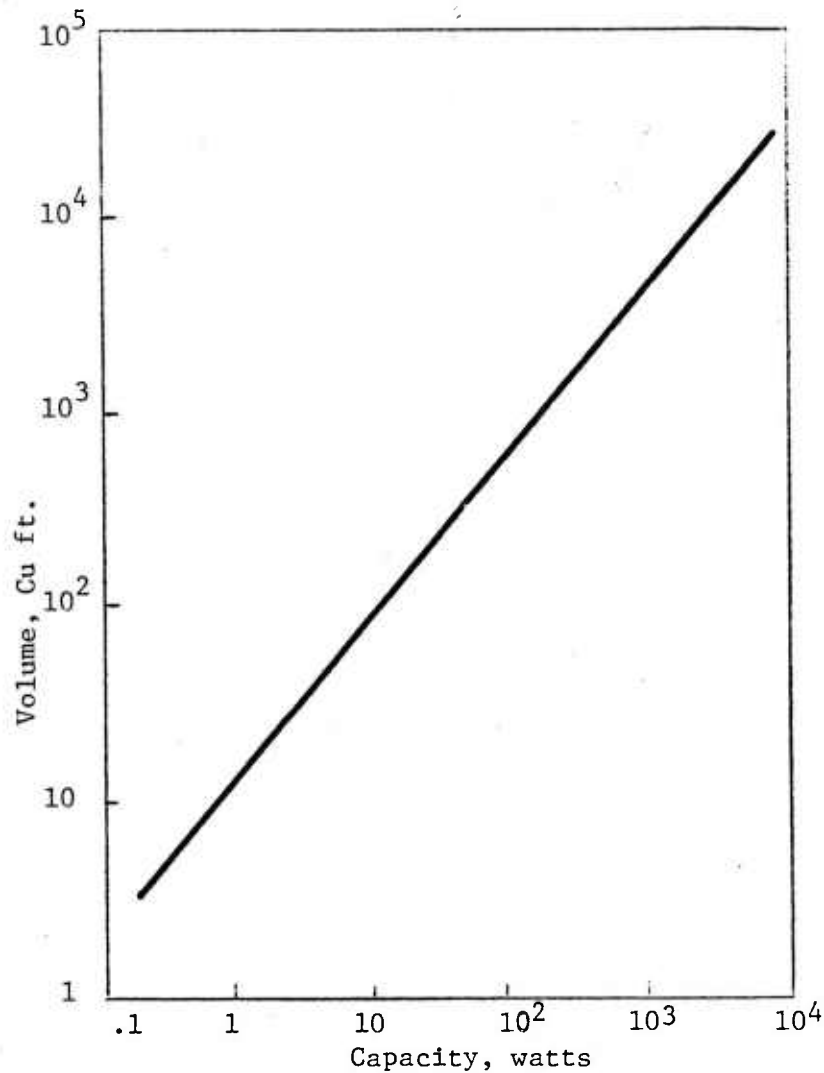


Figure 13. Specify size of refrigerators as a function of their capacity.

Table 4. Summary of some typical sizes

<u>Capacity</u>	<u>Input power per watt of refrig.</u>	<u>Weight per watt</u>	<u>Volume per watt</u>
10-50W	700-1000 W/W	200-300 lbs/W	10 ft ³ /W
1-5W	100-1500 W/W	100-150 lbs/W	5 ft ³ /W

As one would expect it, designs based on different thermodynamic processes yield different specific ratings. Pirtle, et al., (ref 28) made a comparison of three different designs for the same cooling capacity of 25W and for a design goal of 1 kW/W cooling. His findings are summarized in table 5.

Table 5. Comparison of cooling power requirements

<u>Thermodynamic cycle</u>	<u>Weight ratio lb/W (kg/W)</u>	<u>Total volume ft³(m³)</u>	<u>Total power W</u>	<u>Power per W</u>
Collins	180(81.6)	8.5 (0.24)	1762	705
Stirling (Joule-Thomson)	199(90.3)	9.5 (0.26)	2743	1100
Gilford-McMahon (Joule-Thomson)	173(78.3)	9.0 (0.25)	3096	1240

The three reference designs quoted by Pirtle do not give a picture of the advances achieved by manufacturers of larger machines. Table 6 below shows a number of design parameters for refrigerators actually constructed.

Table 6. Design parameters of available refrigerators

<u>Capacity W</u>	<u>Specific power W/W</u>	<u>Weight per W lb/W</u>	<u>Volume per W ft³/W</u>	<u>Ref</u>
14400	878-1094	--	--	
12000	--	5.83	0.408	27
10700	336	--	--	--
1400	429	--	--	--
4	1500	200	1.60	28
225	1333	--	3.78	28
50	877	93	2.32	28

In conclusion, the surveys indicated above show a substantial advance in the performance of the refrigerators manufactured over the past 10 years. Discussions with manufacturers (ref 29) indicate that additional improvement in specific weight and input power is possible and quite conceivable.

Pulsed Sources

Introduction

Most pulsed sources operate on the simple but basic concept of storing energy in a "storage device" and subsequently releasing the stored energy by means of a trigger switch. In most applications of interest, the release has to be very rapid and the transfer of energy from the storage to the recipient "load" must be efficient.

A great deal of research effort has been expended in resolving the issues mentioned above viz., the development of storage systems, of switches and of energy transfer schemes. Although, there exist a great many schemes to store energy, this assessment will concentrate on two that appear to offer many advantages from the point of view of performance and ease of construction. The two schemes referred to are the inductive and inertial storage systems.

We begin by examining some important properties of superconducting inductive systems. In a typical system of this category, we visualize an arrangement such as that shown in figure 14.

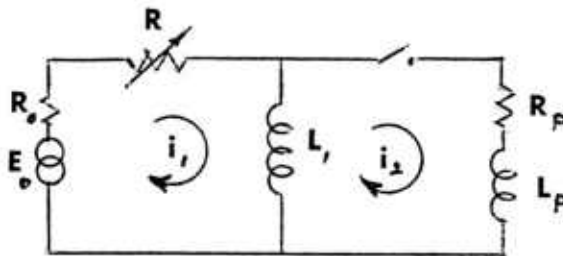


Figure 14. Circuit for transfer from separate inductors

It can be readily shown that i_2 , the current in the load is expressed by

$$i_2(t) = \frac{\alpha_1 \frac{E_o}{R_o} e^{-\frac{\alpha_1}{2} t}}{\sqrt{\frac{\alpha_1^2}{2} - \alpha_1 \alpha_2}} \sinh \sqrt{\left(\frac{\alpha_1}{2}\right)^2 - \alpha_1 \alpha_2} t$$

where $\alpha_1 = (R_o + R_s)/L_p$; $\alpha_2 = \frac{R_p}{L_1}$ and R_s is the resistance of the opening switch that allows the release of energy stored in L , into the load L_p . The switch S is a closing switch. When idle, therefore, it can be represented by an idealized switch.

Now in most cases, $R_o \ll R_s$. Consequently, the time constant $\alpha_1 = R_s/L_p$. To store an appreciable amount of energy $L_1 \ll L_p$. Hence, one finds that

$$\frac{R_s}{L_p} + \frac{R_s}{L_1} \approx \frac{R_s}{L_p}$$

Combining all these approximations in the expression for i_2 , one finds

$$\begin{aligned} i_2(t) &= \frac{E_o}{R_o} \left(\exp\left(-\left(\frac{R_s}{L_p} - \frac{R_p}{L_1}\right)t\right) - \exp\left(-\frac{R_p}{L_1} t\right) \right) \\ &= \frac{E_o}{R_o} \exp\left(-\frac{R_p}{L_1} t\right) \left[\exp\left(\frac{R_s}{L_p} t\right) - 1 \right] \end{aligned}$$

The above expression indicates that the current builds up at a rate dictated mainly by the values of R_s/L_p and decays with a time constant given by R_p/L_1 . The functional dependence of R_s on L_p (or R_p on L_1) for different time constants is shown in figure 15.

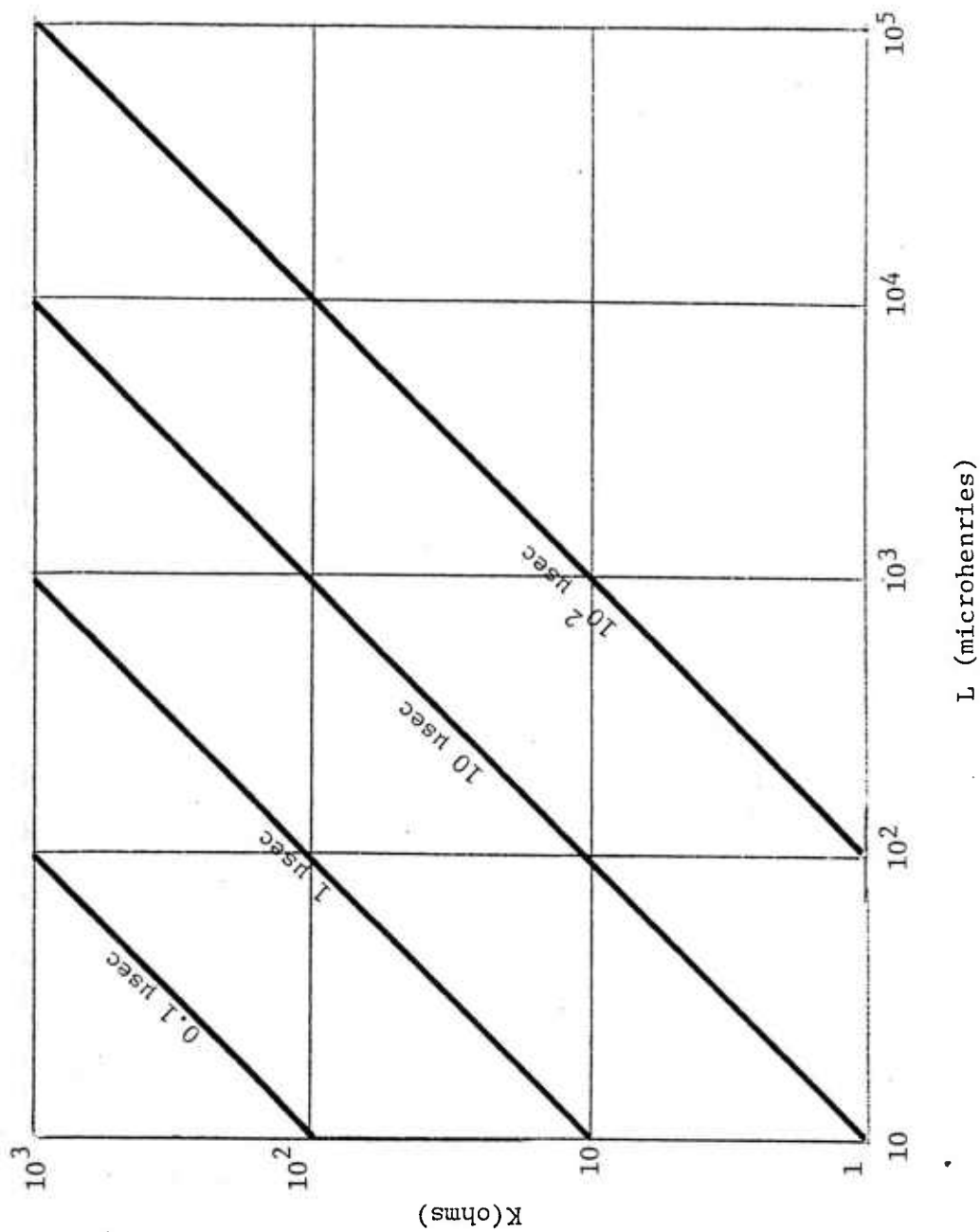


Figure 15. Dependence of the inductance and resistance on the time constant of the coil.

Now, the energy stored is of course $\frac{1}{2} i_1^2(0) L_1$. It becomes apparent that setting a value of 0.1 μsec say, for the sharpness of the pulse, the calculations would indicate that had one chosen $\frac{1}{2} i_1^2(0) L_1 = 10 \text{ MJ}$, and the initial current $i_1(0) = 10 \text{ Kamps}$, $L_1 = 0.2\text{H}$, one would require $R_p = 2 \text{ megohms}$ which is completely unreasonable.

Similarly, selecting a value for R_p in the vicinity of 10 to 100 ohms, one finds that the value of the current becomes unreasonable. To bring down the values of the current and inductance to more realizable figures, a circuit similar to that of figure 16 is suggested.

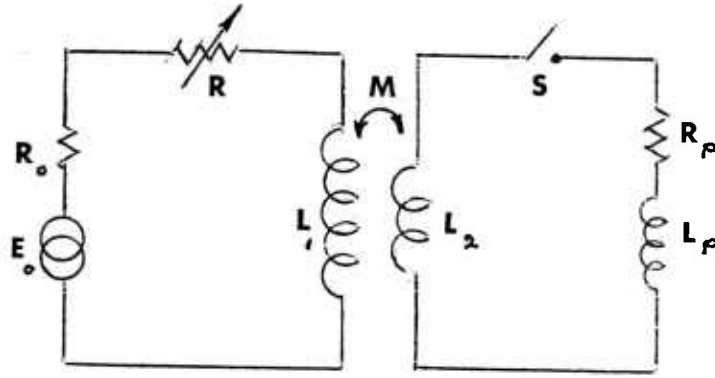


Figure 16. Transfer from transformer coupled inductors.

The insertion of the transformer causes the current in the secondary i.e., in the load to be given by

$$i_2(t) = \sqrt{\frac{L_1}{L_2}} \left(\frac{E_o}{R_o} \right) \left(e^{-\frac{t}{T_h}} - e^{-\frac{t}{T_s}} \right) \frac{T_2}{T_h}$$

In the above formula, $L_2' = L_2 + L_p$; $T_1 = \frac{L_1}{R_s + R_o}$; $T_2 = \frac{L_2'}{R_p}$

and $T_h = T_1 + T_2$; $T_s = \frac{\sigma T_1 T_2}{T_1 + T_2}$

with $\sigma = \frac{L_2 L_1 - M^2}{L_1 L_2}$

For rapid discharges $T_1 \ll T_2$. Consequently

$$T_h \doteq T_2 \quad ; \quad T_s \doteq \sigma T_1$$

Remembering that in addition $L_1 \gg L_2$ the current is expressed by

$$i_2(t) = \sqrt{\frac{L_1}{L_2}} \left(\frac{E_o}{R_o} \right) \left[e^{-\frac{t}{T_2}} - e^{-\frac{t}{\sigma T_1}} \right]$$

showing that the current rises with a characteristic time given by T_s and decays with a constant T_h . The insertion of the transformer allows the current and components to have reasonable values.

As an example if $L_1 = .8\text{mH}$, $L_2' = 2 \mu\text{H}$,

$$\sigma = .05 \text{ (corresponding to 95\% coupling)}$$

and the switch resistance $R_s \rightarrow 10^3$ ohms, then

$$T_1 = \frac{L_1}{R_s} = .8 \mu\text{sec}$$

also

$$T_s = \sigma T_1 = 4 \times 10^{-2} \mu\text{sec}$$

$$T_h \doteq T_2 = \frac{2}{2} = 1 \mu\text{sec}$$

under the assumption that $R_p = 2$ ohms.

Energy Transfer Systems

Introduction

The energy transfer systems discussed in this report are those systems that can be adapted to superconducting pulsed power sources, they need not be superconducting. The operation of these devices rest on energy storages that can be charged or (discharged) in a short time. The nature of the work discussed in this report will concentrate on those systems with times shorter than 1 msec.

Recent advances (ref 30) in applied superconductivity have made inductive energy storage systems very attractive for pulsed power applications. These storages have a definite advantage over conventional systems in cost and size. From stability considerations, the upper limit of the current density in the conductors is somewhere between 5,000 and 10,000 amps/cm² for large coils. The highest obtained field in a large coil has been 15 Teslas. Higher current densities are used at lower fields. The value of 5T is used fairly often. The energy density in superconducting inductive storage systems works out to be about 90J/cm³.

The cost of an inductive energy storage system by comparison to other sources

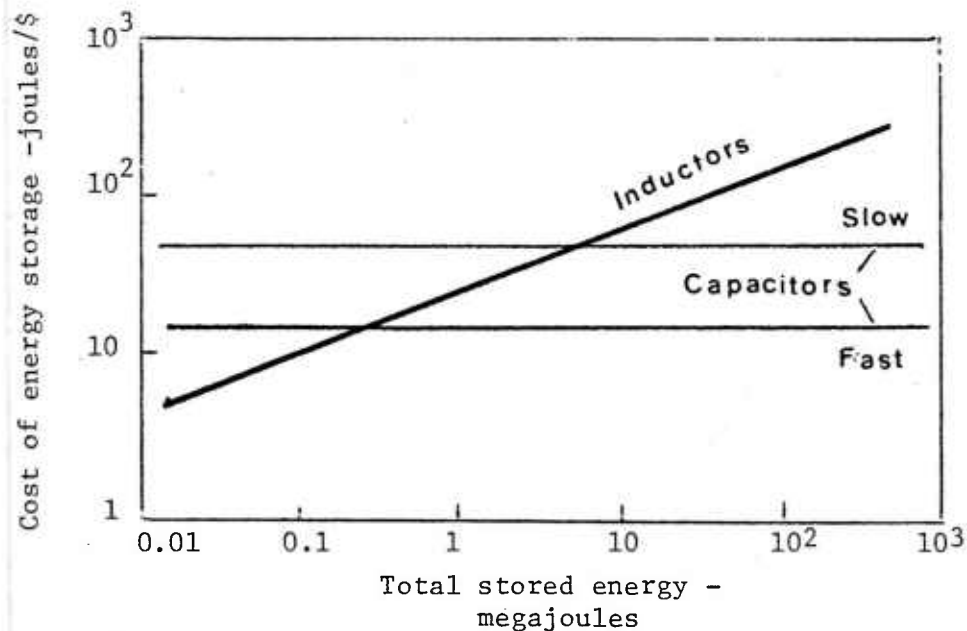


Figure 17. Cost of energy storage vs. current rise time

of energy storage is shown (ref 31) in figure 17 in terms of 1960 (\$). Although the cost has increased, the ranking for the energy stored per unit cost by different schemes remains unchanged.

The superiority of the inductive systems over other storage systems becomes more pronounced when the time constant of the discharge is reduced. Indeed, the stored energy stored per dollar of a normal inductive system is greater than that of a capacitive system for energies greater than 5MJ and greater than that for a pulsed homopolar machine when the time constant is less than 0.1 sec (ref 32) (See fig. 18).

Since the energy density in a superconducting system is one to two order of magnitudes higher than that for a normal system, the expected gain is substantial.

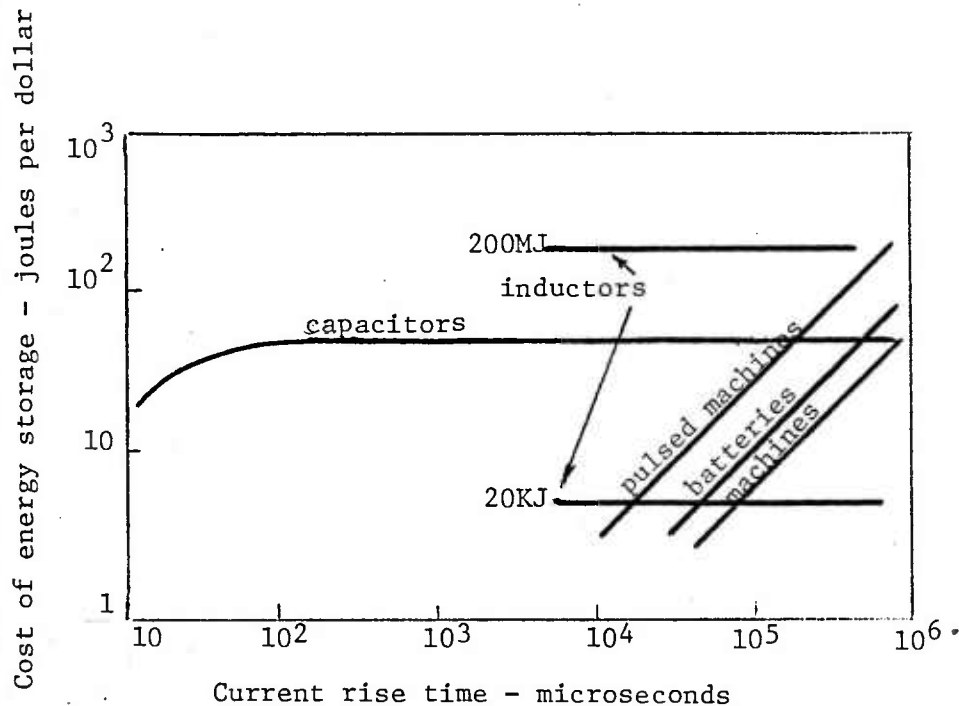


Figure 18. Cost of energy storage vs. current rise time for pulsed system.

The figure 19 (ref 33) shows the weight per unit energy from a number of coils that have actually been constructed. The gain in compactness i.e. Kg per unit of energy improves with size, so does the cost as mentioned above.

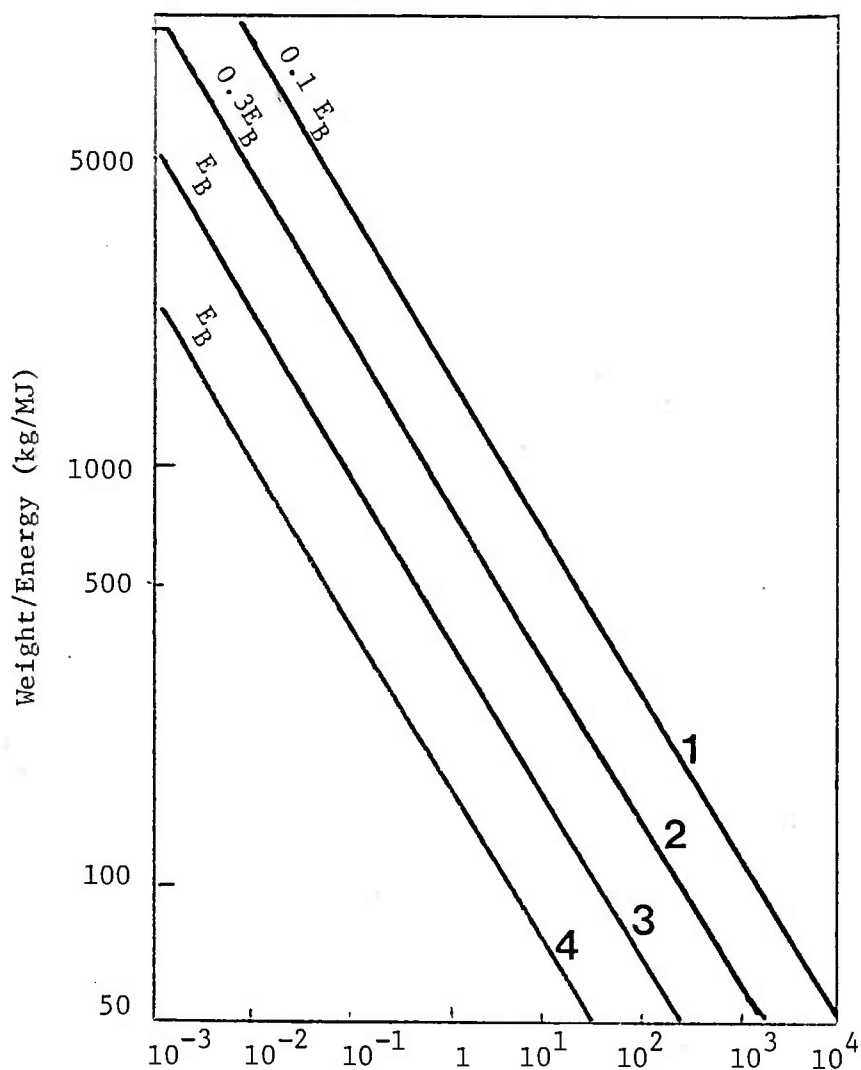


Figure 19. Weight per unit energy of some coils as a function of energy. 1 refers to NbZr wire, 2 and 3 refer to NbTi wire and 4 is for Nb₂Sn wire.

Energy Transfer Mechanisms

The central problem of pulsed inductive energy systems rests on the ability of transferring energy stored in an inductor to a load which is not purely resistive and to perform this operation in a very short time (of the order of several microseconds). This transfer can be accomplished by one of several techniques that have been developed by many investigators. Most of these concepts from a functional point of view can be classified in three groups:

- Group 1. In this class, the energy stored in one or more inductors is transferred to a load inductor by diverting the current from the storage to the load by means of switches. It is assumed that none of the inductors under consideration move or are elastically distorted.
- Group 2. For this group, the energy initially stored in inductors is transferred to the load after an intermediate stage in which the energy in the inductor is first transferred to a capacitor by means of switches and eventually transferred from the capacitor to the inductor. If the capacitor is replaced by a homopolar machine, then, as is well-known, the kinetic energy of the rotor plays the role of an "electrical" capacitance and the two arrangements (capacitance and homopolar) are functionally equivalent.
- Group 3. In this arrangement, the energy stored in one or more inductors is transferred from the storage inductor(s) to the load inductor, without interrupting the current, by altering the shape of the relative positions of the inductors. No capacitors are included in the circuit.

The idealized representation of the three groups is shown below (ref 34) in figure 20.

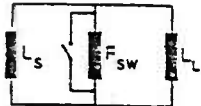
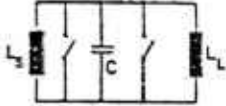
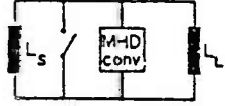
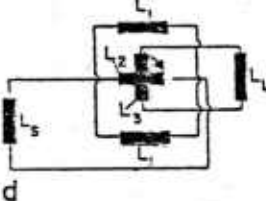
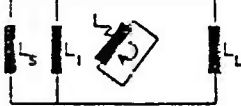
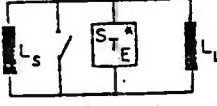
	Transfer element	Ideal efficiency	Other limits
a	Resistor	25%	Switch volume
	Capacitance stationary or homopolar machine	100%	Capacitor Energy: <10 MJ Homopolar capacitor: max forces and torques
	Liquid metal MHD converter	<90%	Losses in the MHD converter
	Rotating inductances (principle motor generator) Mutual inductances $M_{12} \neq 0$, $M_{13} \neq 0$, $M_{23} \neq 0$ For energy transfer from L_s to L_L the system L_2L_3 rotate in L_1 or L_1 rotate around L_2L_3 about 180°	100%	Superconducting moving connexions, torque for inertial energy good mutual inductances $M_{12}M_{13}$
	Coupled rotating inductances	100%	Forces, torques, good mutual inductance M_{12} between the coils of the transfer element
	Stepwise by electronical circuits or reactive elements Stepwise transfer element	$\sim 90\%$	Transfer time, transfer current

Figure 20. Possible transfer circuits for energy cycling between inductive storage and load systems.

REFERENCE DESIGNS

General Remarks

Two designs will be examined in detail. The first will consist of a mass-driver electromagnetic gun associated with a pulsed power source. The source is a superconducting pulsed inductive energy scheme, on the other hand the gun is constructed from normal components. The second design studied consists of the same inductive source used in the first design. This time, however, the shape of the pulse is altered as explained later.

Three classes of guns are of interest. The essential performance goals for these electromagnetic guns are summarized in the table given below.

Table 7. Design criteria for guns

<u>Type of Gun</u>	<u>Mass of projectile</u>	<u>Terminal Velocity</u>	<u>Rate of firing</u>	<u>Length of "barrel"</u>
Heavy	30-70 kg	1 km/sec	2 per min.	4-7.5 m
Medium	5 kg	2.5-3.5 km/sec	6-8 per min.	1 m
Light	30-800 gm	1-1.5 km/sec	10-30 per sec.	3 m

An essential requirement on the first two types is that their life be at least 1000 to 2000 rounds. Also, the weight of the heavy artillery piece should not exceed 30,000 lbs. The life of the light gun should be an order of magnitude greater.

Temporal Character of Source

A question of great interest concerns the relative advantage of starting the projectile impulsively as compared to driving it throughout its travel in the gun.

Two options for the second case are:

- a) the driving force is constant during the motion and b) the force is applied impulsively at periodic intervals.

Case 1. Projectile started impulsively

The starting point of the calculations is Newton's law

$$F = \frac{mdv}{dt} \quad (1)$$

which yields

$$\int F dt = \int m dv$$

If $\Delta\tau$ is the duration of the impulse

$$F\Delta\tau = mv_i \quad (2)$$

i.e., the initial velocity is found from

$$v_i = \frac{F\Delta\tau}{m} \quad (3)$$

But the projectile loses velocity because of losses (friction, aerodynamic,...) in the gun. If we assume that these losses go like the square of the velocity, the equation of motion for projectile is given by

$$m \frac{dv}{dt} = -\alpha v^2 \quad (4)$$

where α is a constant. The above equation integrates to

$$\frac{1}{v} = \frac{1}{v_i} + \frac{\alpha}{m} t \quad (5)$$

The functional dependence for the position of the projectile in the gun as a function of time, can be readily found from (4) by using the relation

$$v = \frac{dx}{dt} \quad (6)$$

In the above, x is the position of the projectile measured from the breech of the gun. Combining (5) and (6) one finds

$$\frac{dt}{dx} = \left(\frac{1}{v_i} + \frac{\alpha}{m} t \right) \quad (7)$$

The solution of equation (7), yields

$$t = \frac{m}{\alpha v_i} (e^{\frac{\alpha}{m} x} - 1) \quad (8)$$

Using (5) and (8) one computes readily that in order for the projectile to exit with a velocity v_e when it reaches the muzzle of gun where $x = L$, one should start with a velocity v_i such that

$$\begin{aligned} (v_i)^{-1} &= \frac{1}{v_e} - \frac{\alpha}{m} (e^{\frac{\alpha}{m} L} - 1) \frac{m}{\alpha v_i} \\ &= (v_e)^{-1} - (v_i)^{-1} (e^{\frac{\alpha}{m} L} - 1) \end{aligned}$$

i.e.

$$v_i = v_e (e^{\frac{\alpha}{m} L}) \quad (9)$$

The energy of the impulse is

$$W_e = \frac{mv_i^2}{2} = \left(\frac{F \Delta \tau}{2m} \right) = \frac{m}{2} v_e^2 (e^{\frac{2\alpha}{m} L}) \quad (10)$$

Case 2. Projectile Driven with Constant Force

For this case, the governing equation for the motion of the particle is

$$F = m \frac{dv}{dt} + \alpha v^2 \quad (11)$$

The solution of this equation is

$$v = \left(\frac{F}{\alpha} \right)^{1/2} \left(1 - \frac{m}{m - (\alpha F)^{1/2} t} \right) \quad (12)$$

The variation of the velocity with the distance can be deduced from the above equation as follows:

$$v = \frac{dx}{dt} = \left(\frac{F}{\alpha} \right)^{1/2} \left(1 - \frac{m}{m - (\alpha F)^{1/2} t} \right), \quad (13)$$

where the integration

$$x = \left(\frac{F}{\alpha}\right)^{1/2} t - \frac{m}{\alpha} \ln \left(1 - \frac{(\alpha F)^{1/2}}{m} t\right) \quad (14)$$

The above satisfies the initial condition $x \rightarrow 0$; $t \rightarrow 0$

The dependence of the velocity of the projectile on the distance is found directly from (11), by means of the transformation

$$\begin{aligned} F &= m \frac{dv}{dt} + \alpha v^2 = m \frac{dv}{dx} \frac{dx}{dt} + \alpha v^2 \\ &= \frac{1}{2} m \frac{dv^2}{dx} + \alpha v^2 \end{aligned} \quad (15)$$

This yields at once

$$v^2 = \frac{F}{\alpha} \left(1 - e^{-\frac{2\alpha}{m} x}\right) \quad (16)$$

The energy expended is $W_e = FL$. As a function of the velocity v_e this energy is

$$v_e^2 = \left(\frac{FL}{\alpha L}\right) \left(1 - e^{-\frac{2\alpha L}{m}}\right)$$

or

$$W_e = \frac{mv_e^2 \frac{2\alpha L}{m}}{2(1 - e^{-\frac{2\alpha L}{m}})} \quad (17)$$

Case 3. Projectile Accelerated by Succession of Pulses

For this particular situation, a number of impulses are imparted to the projectile while it travels down the gun. If we assume that the impulses are produced n times at at equally distant locations: $0, \frac{L}{n}, 2 \frac{L}{n}, \dots, (\frac{n-1}{n})L$, the velocity histogram of the projectile is found as follows.

In the interval $0 < x < \frac{L}{n}$, the velocity is given by Equation (5) and input energy by Equation (10). Similarly, between $x = \frac{L}{n}$ and $x < \frac{2L}{n}$

$$v = v_1 e^{-\frac{\alpha}{m} x} \left(1 + e^{-\frac{\alpha L}{mn}}\right) \quad (18)$$

In equation (18) it was assumed, that an impulse equal to (mv_i) was applied at $x = \frac{L}{n}$. It is easy to show that the exit velocity of the projectile is

$$v_e = v_i e^{-\frac{\alpha L}{m n} (1 + e^{-\frac{\alpha L}{m n}} + e^{-\frac{2\alpha L}{m n}} + \dots + e^{-\frac{(n-1)\alpha L}{m n}})}$$

$$= v_i e^{-\frac{\alpha L}{mn} (n - \frac{\alpha L}{2m})} \quad \text{if } n \text{ is large} \quad (19)$$

The energy input to the gun is $n^2 \frac{mv_i^2}{2}$ which by means of (19) can be written as

$$W_e = \frac{mv_e^2}{2} e^{\frac{2\alpha L}{mn} (1 + \frac{\alpha L}{mn})} \quad (20)$$

When one compares the three cases discussed above, then for identical exit velocities the energy requirement will be in the ratios of

$$(e^{\frac{2\alpha L}{m}}) :: \frac{2\alpha L}{m} \frac{1}{(1 - e^{-\frac{2\alpha L}{m}})} :: e^{\frac{2\alpha L}{mn} (1 + \frac{\alpha L}{mn})}$$

The functional behavior of these ratios is shown in graphical form in fig. 1 for $N = 10$. The advantage of case 3. is clearly demonstrated.

Outline of Design I

The main features of this design which will be referred to as the "A" system is summarized by the bloc diagram shown below.

The proposed gun consists of a repulsion coil arrangement in which the moving coil C i.e. the "projectile" is guided by rails. The rails double-up as mechanical guides and as bus bars through which a current can be fed to the coil C.

The current to the main driving coils L_1, L_2, \dots is generated by a pulsed source S. The main pulse from S is fed to a transmission line (TL). As a result of the propagation of the pulse down the line the current to C_1, C_2, \dots coils located on

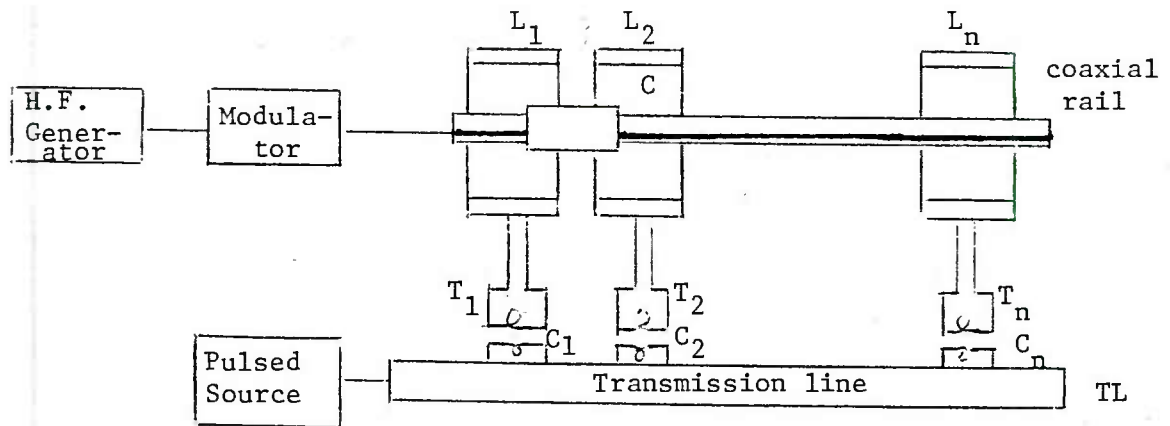


Figure 21. Block diagram for synchronous accelerator.

the line - arrives sequentially. These currents after appropriate transformation are fed to the driver coils L_1, L_2, \dots .

The combination of transformers (T_1, T_2, \dots) and transmission line makes it possible to excite the driver coils at the appropriate time without the use of any switching device.

It is essential to design the transmission so that the main pulse - from S - travels down the line in synchronism with the coil C. This is readily achieved by matching the two speed (i.e. that of the pulse and that of C) approximately. Fine adjustment for synchronism is secured through the modulator in the manner described below.

The design procedure will begin with a study of the interior ballistics of the gun. Having determined the necessary requirement for the gun, attention will be directed in turn to the transmission line needed and to the energy sources.

Interior Ballistics of Gun

The derivation for the dynamics of the projectile in the gun is much easier to obtain by means of piece-wise solutions. Each one of these solutions will treat the passage of the projectile into one coil. The general solution for the behavior of the projectile throughout the gun is then constructed by piecing elementary solutions through a match at the exit of one coil and inlet at the neighboring coil.

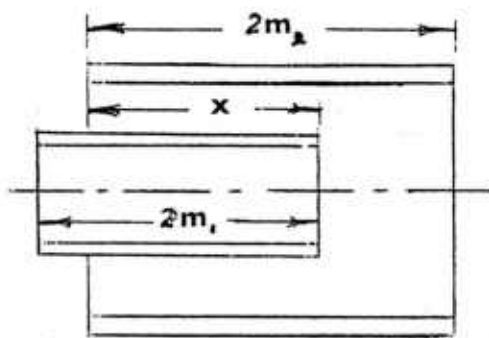


Figure 22. Geometry of driver and driven coils.

Let us consider the r^{th} coil L_r in which circulates a current I_r . Let this coil be of length $2m_2$ (fig.22) while the projectile coil C be assumed to have a length $2m_1$. If we denote by "x" the displacement of C inside L_r , then conservation of momentum requires that

$$m \frac{dv}{dt} + \alpha v^n = I_r I_o \frac{\partial L_{ro}}{\partial x} \quad (21)$$

As before α is related to the friction losses of the projectile (windage, solid friction contributed by the sabot,...), m is the mass of the projectile, L_{ro} is the mutual inductance between L_r and C , I_o is the current in C , while n is an index which is equal to unity at low speeds and climbs to a value near to two as the projectile picks up speed. To simplify the algebra we will choose n to be equal to one. Later,

we will derive the necessary correction as n approaches the value of 2.

A second relation for the motion of the projectile is found from the circuit equivalent, that reflects the back emf reflected on the source as a result of the motion.

This equation is

$$L_{rr} \frac{dI_r}{dt} + v I_o \frac{\partial L_{ro}}{\partial x} + R_{rr} I_r = E_r(t) \quad (22)$$

In the above, L_{rr} stands for the self inductance of the r^{th} coil, R_{rr} for its ohmic resistance and $E_r(t)$ is the voltage across L_r .

Now it was shown (ref 35) that the driving force $I_r I_o \frac{\partial L_{ro}}{\partial x}$ depends strongly on the ratio m_2/m_1 . It turns out that this force is a maximum for $m_2 \approx m_1$. For this reason, the coils will be so constructed. Since L_{ro} obviously does not depend on the time, the two simultaneous equations are solved by means of Fourier transforms. Accordingly, we first eliminate I_r between equations (21) and (22).

We thus find

$$\begin{aligned} \frac{d^2 v}{dt^2} + \left(\frac{\alpha}{m} + \frac{R_{rr}}{L_{rr}} \right) \frac{dv}{dt} + \left(\frac{\alpha}{m} \frac{R_{rr}}{L_{rr}} + \frac{1}{L_{rr} m} \left(I_o \frac{\partial L_{ro}}{\partial x} \right)^2 \right) v \\ = \frac{I_o}{m L_{rr}} \left(\frac{\partial L_{ro}}{\partial x} \right) E_r \end{aligned} \quad (23)$$

Introducing the transforms

$$\begin{aligned} \tilde{v} &= \frac{1}{\sqrt{2\pi}} \int_{-\infty}^{\infty} v(t) e^{-i\omega t} dt \\ \tilde{I}_r &= \frac{1}{\sqrt{2\pi}} \int_{-\infty}^{\infty} I_r(t) e^{-j\omega t} dt \\ \tilde{E}_r &= \frac{1}{\sqrt{2\pi}} \int_{-\infty}^{\infty} E_r(t) e^{-i\omega t} dt \end{aligned} \quad (24)$$

we find at once

$$\begin{aligned} \tilde{v}(\omega) & \left[\left(\frac{\alpha}{m} \frac{R_{rr}}{L_{rr}} + \frac{1}{mL_{rr}} \left(I_o \frac{\partial L_{ro}}{\partial x} \right)^2 \right) - \omega^2 + i\omega \left(\frac{\alpha}{m} + \frac{R_{rr}}{L_{rr}} \right) \right] \\ & = \frac{I_o}{mL_{rr}} \left(\frac{\partial L_{ro}}{\partial x} \right) \tilde{E}_r \end{aligned} \quad (25)$$

The inverse transform of (25) leads to

$$v(t) = \frac{1}{\sqrt{2\pi}} \int_{-\infty}^{\infty} \frac{\tilde{E}_r(\omega) e^{i\omega t} a(x) d\omega}{(mL_{rr} a^2 + \frac{\alpha}{m} \frac{R_{rr}}{L_{rr}}) - \omega^2 + L\omega \left(\frac{\alpha}{m} + \frac{R_{rr}}{L_{rr}} \right)} \quad (26)$$

The symbol $a(x) = \frac{I_o}{mL_{rr}} \left(\frac{\partial L_{ro}}{\partial x} \right)$ is independent of time and is approximated by a rectangular stepwise function. If one also assumes $E_r(t)$ to be an impulse voltage, the equation (26) is evaluated to be

$$v(t) = \frac{1}{\sqrt{2\pi}} E_o \frac{I_o}{mL_{rr}} \left(\frac{\partial L_{ro}}{\partial x} \right) \frac{e^{-p_1 t} - e^{-p_2 t}}{\sqrt{\left(\frac{\alpha}{m} - \frac{R_{rr}}{L_{rr}} \right)^2 + 4mL_{rr} a^2}} \quad (27)$$

If $4mL_{rr} a^2 \gg \left(\frac{\alpha}{m} - \frac{R_{rr}}{L_{rr}} \right)^2$, then

$$\begin{aligned} v(t) & = \frac{1}{\sqrt{2\pi}} E_o \frac{e^{-\left(\frac{\alpha}{m} + \frac{R_{rr}}{L_{rr}} \right) \frac{t}{2}} [i \sin a \sqrt{mL_{rr}} t]^2}{i \sqrt{4mL_{rr}}} \\ & = \frac{1}{\sqrt{2\pi}} E_o e^{-\left(\frac{\alpha}{m} + \frac{R_{rr}}{L_{rr}} \right) \frac{t}{2}} \frac{\sin(a \sqrt{mL_{rr}} t)}{\sqrt{mL_{rr}}} \end{aligned} \quad (28)$$

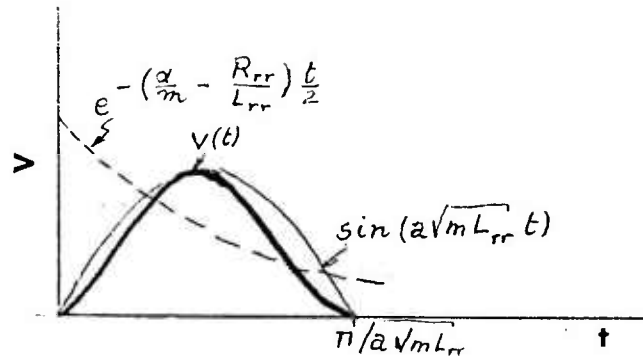


Figure 23. Functional dependence of $v(t)$

where $a\sqrt{mL_{rr}} = \frac{I_0}{\sqrt{mL_{rr}}} \left(\frac{\partial L_{ro}}{\partial x} \right)$.

We have to design the system such that $\frac{I_0}{\sqrt{mL_{rr}}} \left(\frac{\partial L_{ro}}{\partial x} \right) = \frac{\pi}{2}$ (fig. 24)

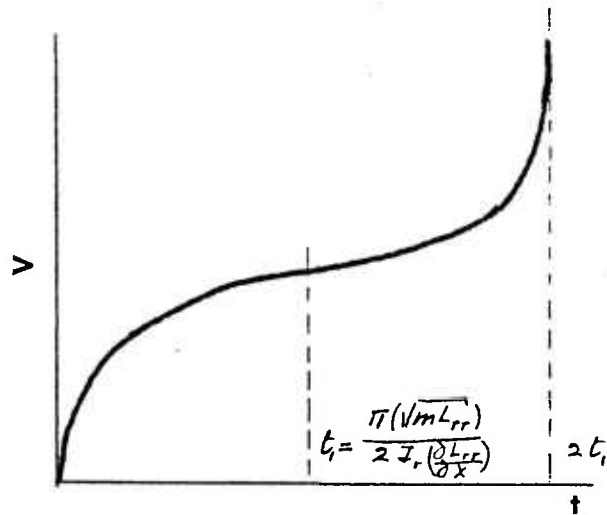


Figure 24. Forces appearing on coil over one full traverse

The projectile is midway the coil at $t = t_1$. At this point, I_r must be reversed, so that the velocity continues to increase. Except for the damping we can find the variation of the displacement from

$$v(t) = \frac{dx}{dt}$$

Consequently

$$x = \int v(t) dt = \frac{1}{\sqrt{2\pi}} E_0 \int e^{-\left(\frac{\alpha}{m} + \frac{R_{rr}}{L}\right)t} \frac{\sin(\sqrt{mL_{rr}} t)}{\sqrt{mL_{rr}}} dt \quad (29)$$

The integration of equation (29) yields

$$x = \frac{E_0}{\sqrt{2\pi}} \frac{\left(\frac{\alpha}{m} + \frac{R_{rr}}{L}\right)}{\sqrt{mL_{rr}}} e^{-\left(\frac{\alpha}{m} + \frac{R_{rr}}{L}\right)t} \quad (30)$$

$$x = \frac{\sin(\sqrt{mL_{rr}} t - \left(\frac{\alpha}{m} + \frac{R_{rr}}{L}\right)t)}{\left(\left(\frac{\alpha}{m} + \frac{R_{rr}}{L}\right)^2 - mL_{rr}\right)}$$

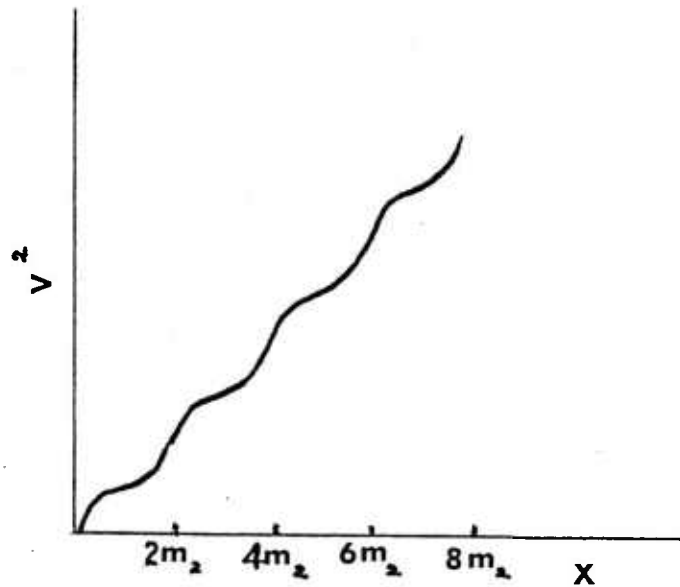


Figure 25. Dependence of the velocity on the position of the projectile.

Propagation of Transient on Transmission Line

Since the transmission line is dispersive, we need to look carefully to the evolution of the signal $E(\omega)$ down the line. The line actually can be represented by a chain of quadrupoles, all similar to those shown in figure 26.

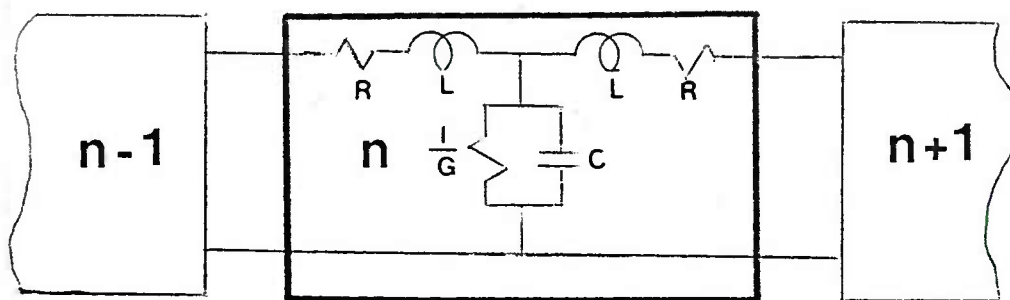


Figure 26. Typical circuit used in the transmission line lattice.

The resistances R & $\frac{1}{G}$ represent the losses both in the coil and in the transfer of energy to the gun.

The solution of the transient, when a unit impulse is applied to the chain has actually been derived in Campbell & Foster's Fourier Integrals (ref 36).

In this formula, if we take $\sqrt{\frac{L}{C}} = k$; $\frac{R}{L} = \frac{G}{C} = \lambda$; $\frac{2}{\sqrt{LC}} = \omega$ then the response at the output of the n th quadrupole is $\frac{2}{L} e^{-\lambda t} J_{2n}(\omega t)$. The graphical representation for the first five locations is shown in figure 27.

Characteristics of Pulsed Sources

The proposed pulse source consists of a superconducting storage inductor, a current source (flux pump) and a superconducting switch.

The energy stored in the inductor will be extracted from the coil through a transformer inductively coupled to the storage coil. To minimize the thermal losses, the secondary of the transformer is kept outside the cryostat.

Before the construction details of the source are discussed, the governing parameters for the pulsed source are calculated. The results are summarize in table 3.

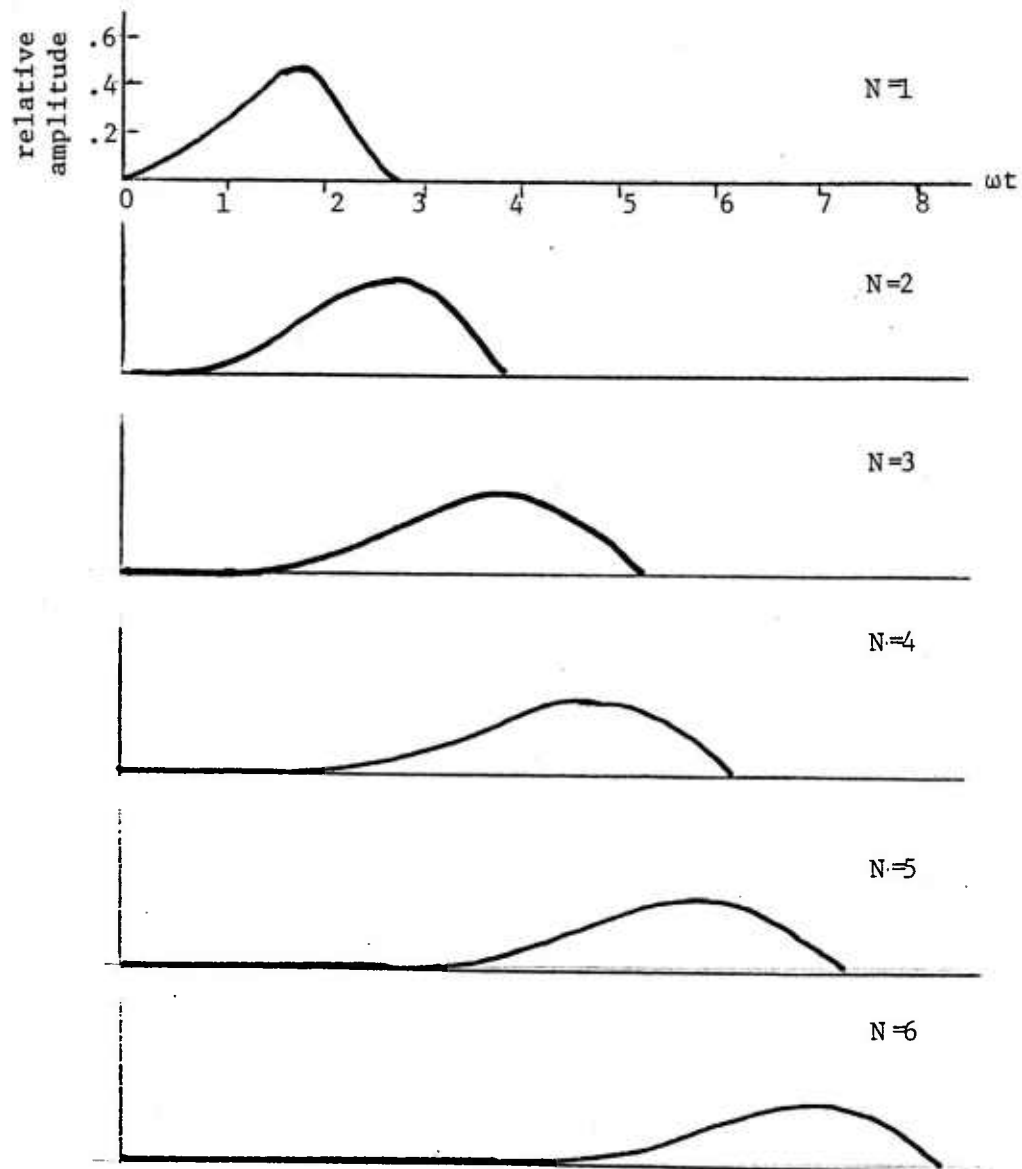


Figure 27. Evolution of pulse down the gun

Table 8. Inductance needed for various pulses

<u>Energy/pulse</u>	<u>Current</u>	<u>Storage inductance</u>
15 MJ	10^4	700 mH
15 MJ	10^4	300 mH
1 MJ	5×10^3	80 mH
15 kJ	5×10^3	1.2 mH

From circuit theory consideration

$$L \frac{dI}{dt} = V \quad (31)$$

or

$$I = \frac{V}{L} t$$

(when the coils is charged at constant voltage).

Consequently, one finds by means of the previous table the following charging times:

Table 9. Charging times for various gun ratings

<u>Type of gun</u>	<u>Energy/pulse</u>	<u>Current</u>	<u>Voltage</u>	<u>Charging time</u>
Heavy	35 MJ	10^4	233	30 sec.
Medium	15 MJ	10^4	300	10 sec.
Light	1 MJ	5×10^3	2000	0.2 sec.
Light	15 kJ	5×10^3	30	0.2 sec.

For the case of the light guns, the charging time is too long [Specs call for firing 10-30 rounds/sec]. So, for the one IMJ pulsed source one finds

Table 10. Source characteristics needed for various inductors

<u>Charging voltage (volts)</u>	<u>Charging current (amps)</u>	<u>Charge time</u>	<u>Inductance</u>
2000	5×10^3	0.2 sec.	80 mH
1264	15.8×10^3	0.1 sec.	8 mH
400	50×10^3	0.1 sec.	0.8 mH

SUMMARY OF DATA
Table 11

Type of Gun	Mass of projectile	Muzzle velocity km/sec	Energy per pulse MJ	Repetition Rate	Current amps	Voltage volts	Charging time	Inductance (Henries)	Energy loss	No. of Pump for 200w
Heavy	50 kg (30 to 70kg)	1km/sec	25	2/min.					1%	
Medium	5 kg	2.5-3.5 km/sec 3 km/sec	(16.6 to 30.6) 22.5	6 to 8/min						
Light	30-800 gm	3 km/sec 1→ 1.5)	(.135 to 3.6) (.015 to .4)	10 to 30 sec.						
Options										
Heavy		1 km/sec	35	2 min	10 ⁴	233	30 sec	700	11.7Kw 1.17 Kw	~ 6
					1.5x10 ⁴	155	30 sec	311		
					5x10 ⁴	45.7	30 sec	28		
Medium		3 km/sec	30	6/min	10 ⁴	600	10 sec	600	30Kw 3.0Kw	~ 15
					1.5x10 ⁴	400	10 sec	266.7		
					5x10 ⁴	120	10 sec	24		
Light		3 km/sec	.40	10/sec	10 ⁴	800	0.1 sec	.8	40Kw 4Kw	20
			.015	10/sec	10 ⁴	80	0.1 sec	0.8	1.5Kw 15Kw	
					1.5x10 ⁴	20	0.1 sec	0.133	-- --	
					5x10 ⁴	6	0.1 sec	0.012	-- --	
			.40		5x10 ⁴					

Storage Coil

It is well-known (ref 37) that a Brooks' coil provides the optimum utilization of conductors per unit energy sotred in the coil. Unfortunately, cylindrical coils have a substantial fringe field. Radiation from the coil when pulsed can be serious.

The use of a toroidal coil on the other hand, will not suffer from the drawbacks mentioned above. But the use of conductors is not optimized. A trade-off is, therefore, obtained between these two features.

Now the inductance of a toroidal coil of rectangular cross-section can be found from energetic arguments or from classic arguments of electromagnetic theory (ref 38).

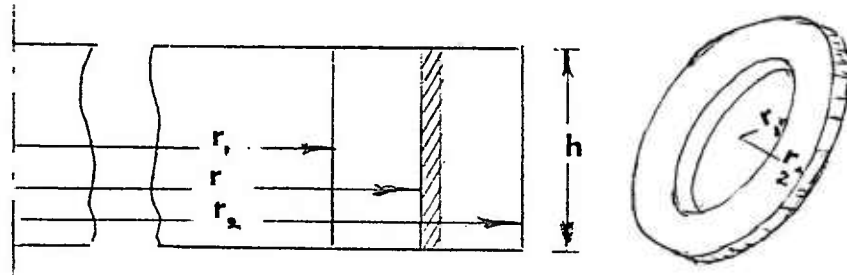


Figure 28. Dimensions of toroidal storage coil.

Let us start with the first argument. The magnetic flux density in the coil is given by

$$B(r) = \frac{B_o r_1}{2\pi r} \quad (B_o \text{ max field at } r=r_1) \quad (32)$$

Consequently the energy stored in the coil is

$$\begin{aligned} E_m &= \frac{1}{2\mu_o} \int B^2 dv \\ &= \frac{1}{2\mu_o} \int_0^{2\pi} \int_{r_1}^{r_2} \frac{B_o^2 r_1^2 dv h}{(2\pi r)^2} = \frac{\pi B_o^2 h r_1^2 \ln \frac{r_2}{r_1}}{\mu_o} \end{aligned} \quad (33)$$

But it is known that the aspect ratio of the torus that will optimized the use of material (ref 39), is that for which

$$\frac{r_2 - r_1}{2} = \frac{1}{3} \left(\frac{r_2 + r_1}{2} \right) \quad (34)$$

This yields at once

$$r_1 = \frac{r_2}{2} \quad (35)$$

Consequently, the previous relation becomes

$$E = \frac{B_o^2 r_1^3 \ln 2}{4 \times 10^{-7}} \quad (36)$$

The graphical representation of this relation is shown in figures 29 and 30. Since

$$E = \frac{1}{2} Li^2 \quad (37)$$

we derive L at once, provided i is fixed. We will choose $i = 5 \times 10^4$ amps. (fig. 31).

The other relation for the coil is that derived by Grover (ref 40). It actually is

$$L = 0.002 N^2 h \log \frac{r_2}{r_1} - 0.002 N (G+H) \quad (38)$$

In the above

$$e = 2(h + (r_2 - r_1)) \text{ cm} \quad (39)$$

while G & H are functions tabulated in Grover (ref 40).

Conductors Characteristics

The construction of the coil is considerably simplified if one uses internally cooled cabled superconductors (ICCS). The ICCS provides its own helium cryostat. Furthermore, the stainless steel encapsulated ICCS can be fully insulated. This is a most desirable feature in view of the high voltages which will be developed in the coil.

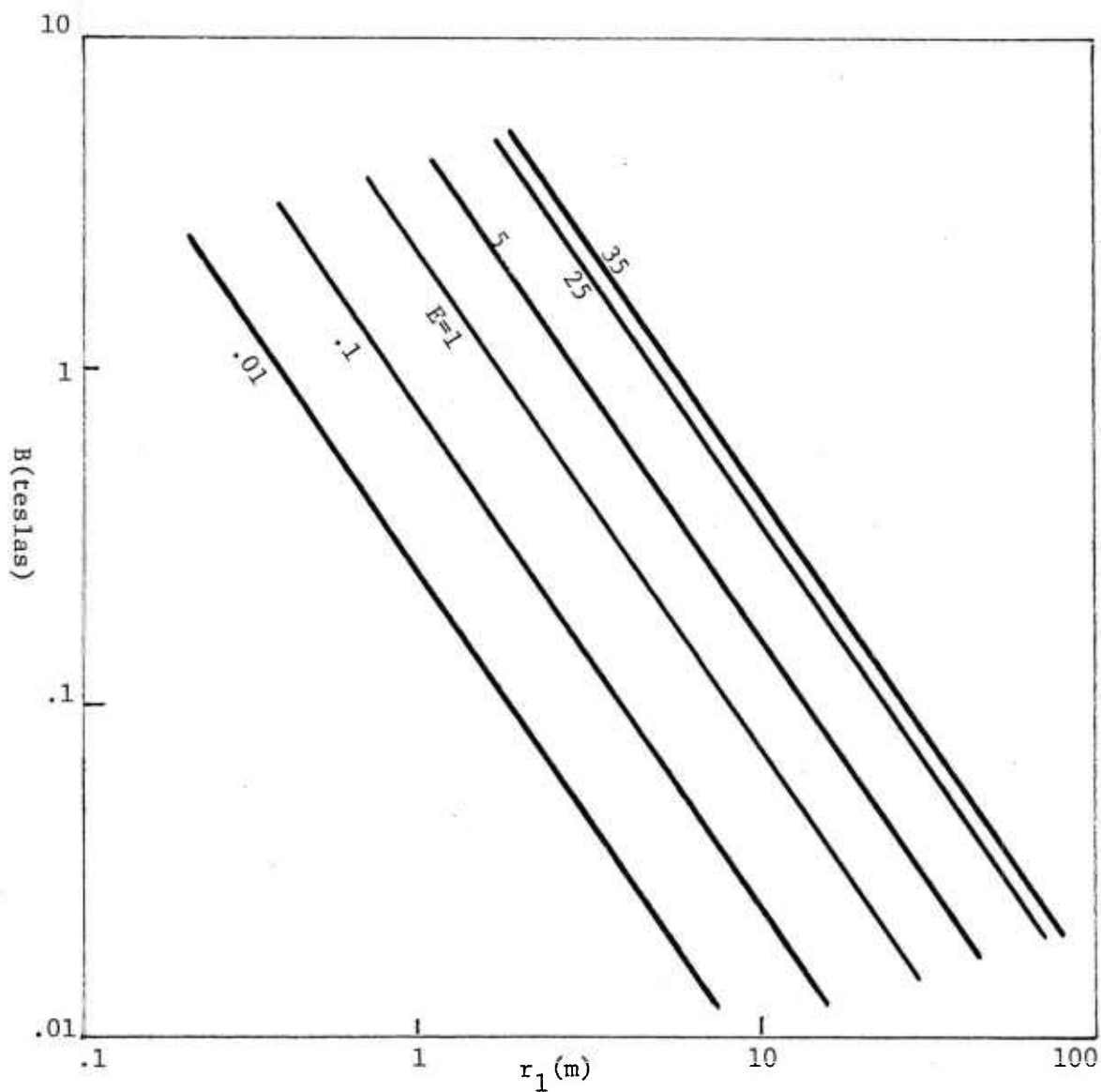


Figure 29. Dependence of the magnetic field on the size of the torus and on the energy stored.

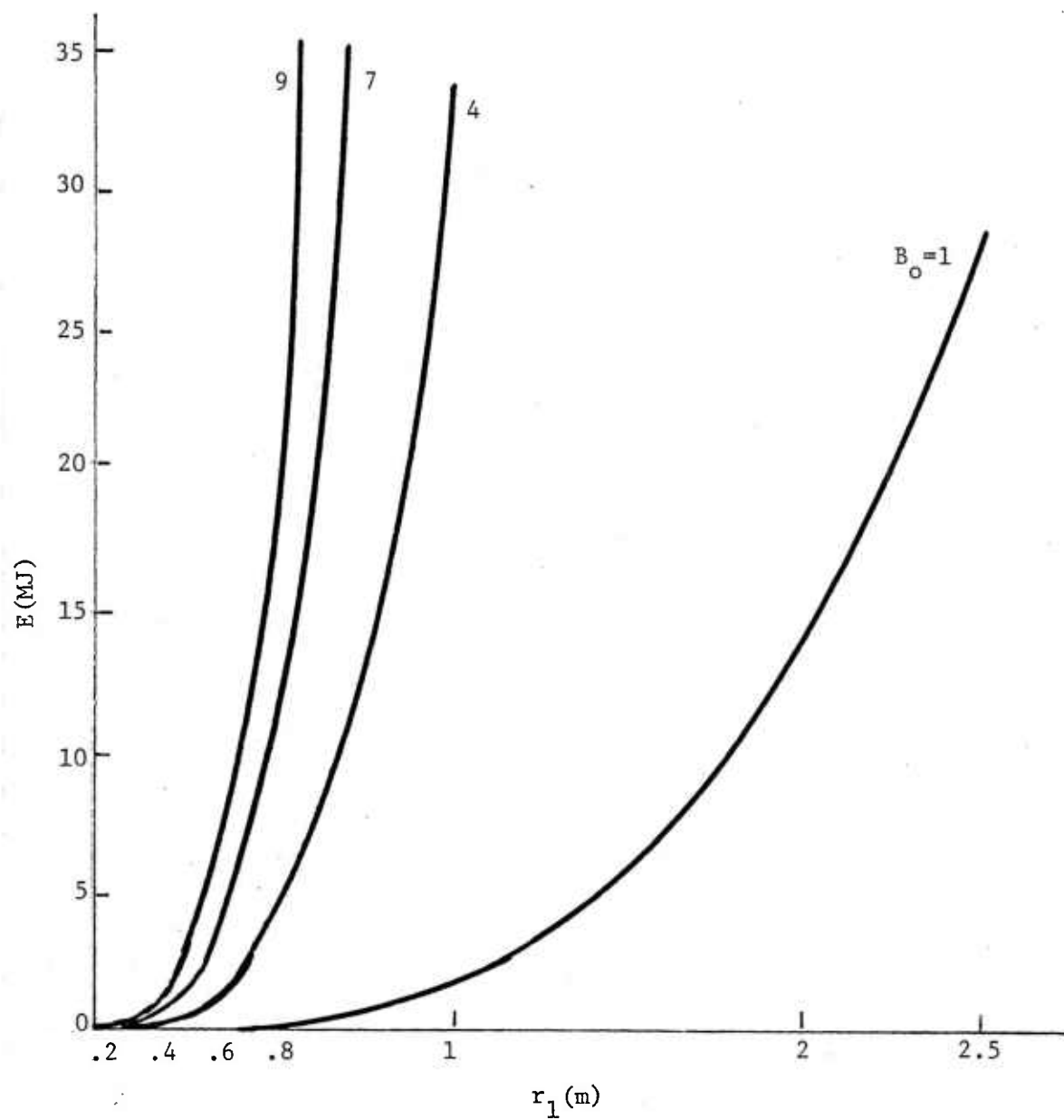


Figure 30. Dependence of the energy stored on the maximum field used.

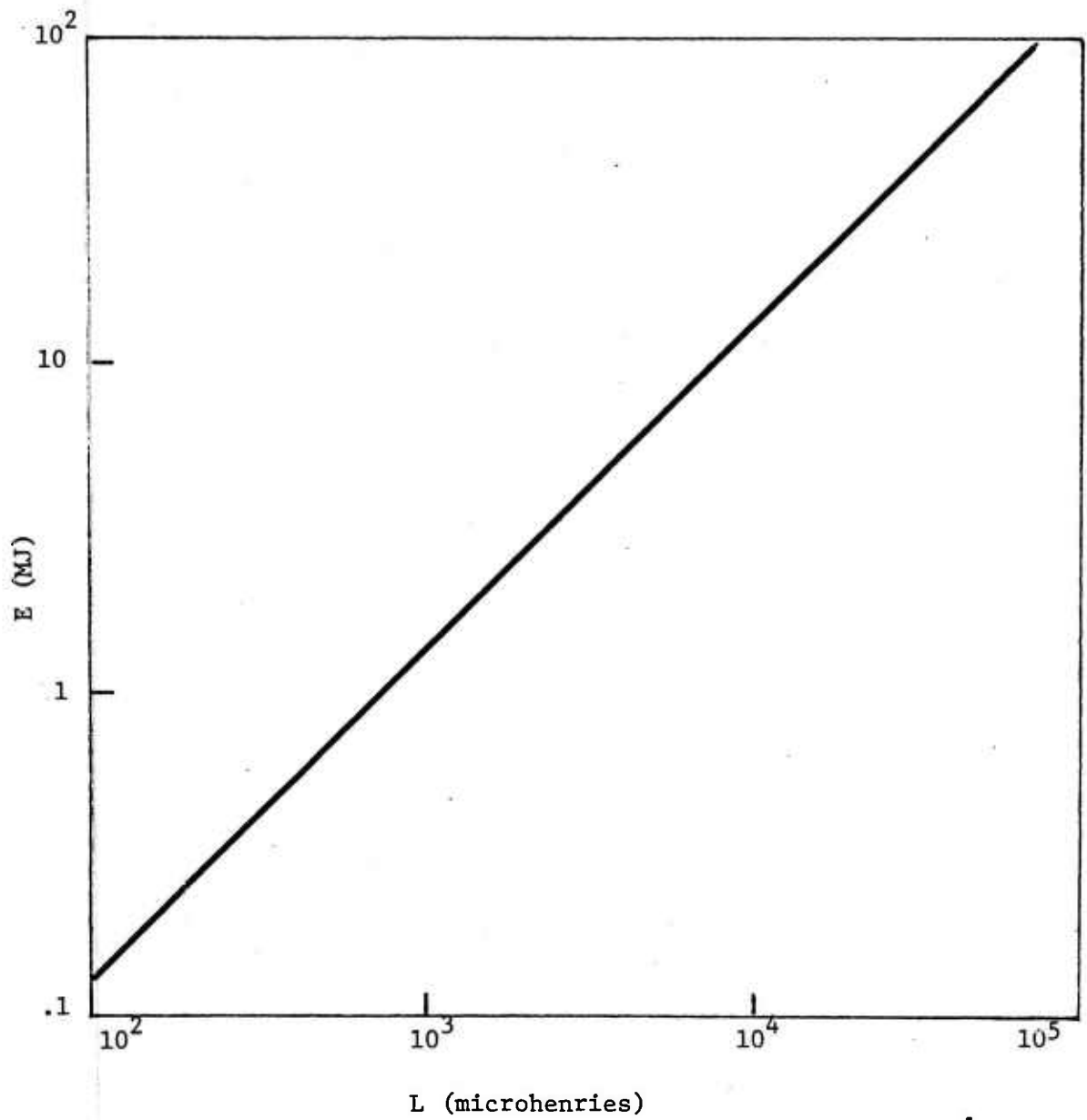


Figure 31. Dependence of the energy on the inductance of the storage coil.

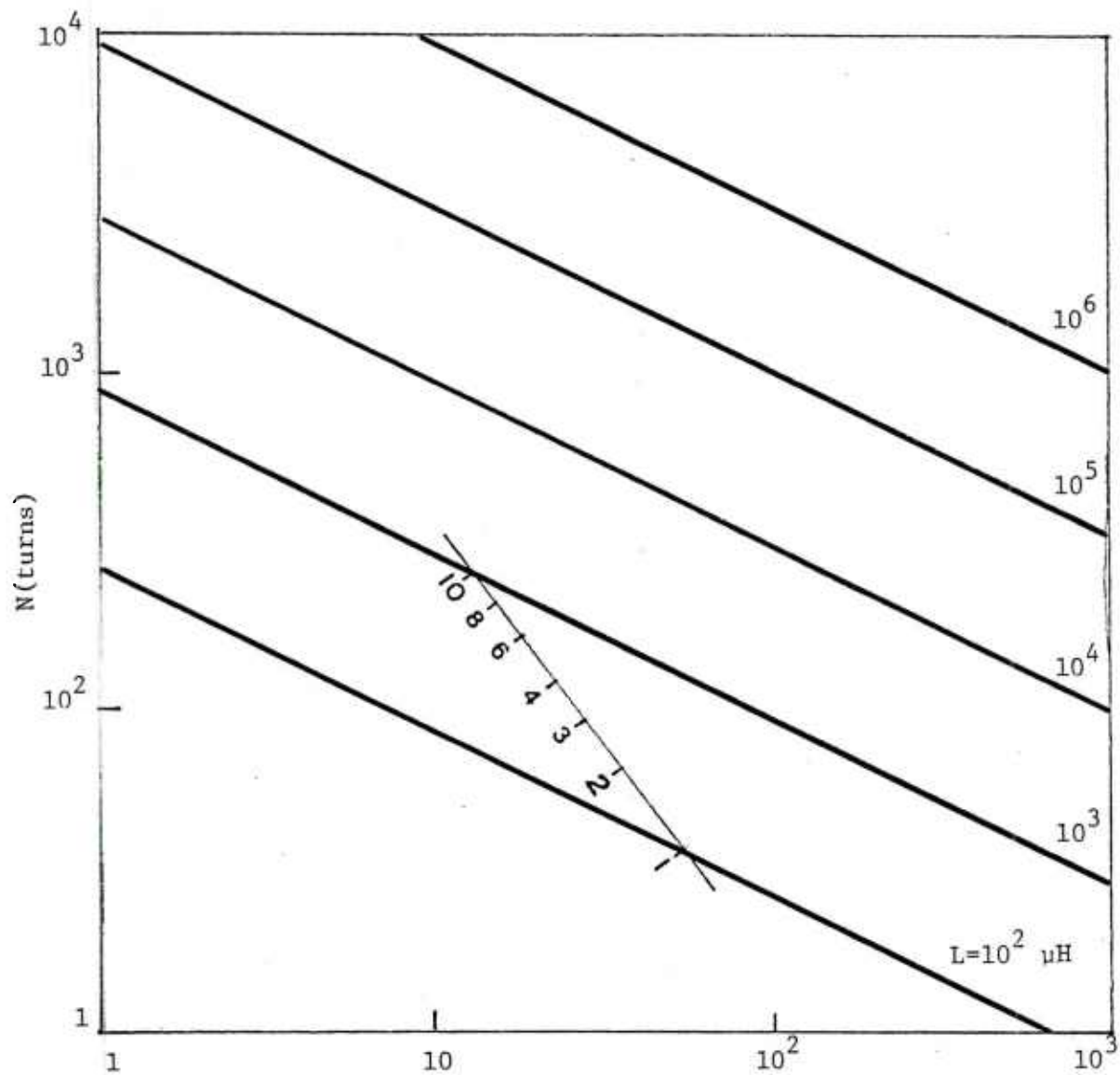


Figure 32. Nomograph for the coil parameters.

The stainless steel jacket of the ICCS can be tailored to withstand the severe magnetic forces in the coil. Large, vertical, pool boiling helium cooled superconducting coils must be adequately ventilated to protect their superconductors from low density vapor. ICCS, on the other hand, are free from orientation constraints.

The conductors proposed to be used in our reference design are similar to those considered in two independent studies on the feasibility of ICCS (ref 41). Experimental verifications of these conductors lends credibility to their projected performance. Their characteristics are summarized in the table shown below.

Table 12. Conductor characteristics

Peak field (Tesla)	9
Type of conductor	Braid
S/C material	Nb ₃ S _n
Number of strands	503
Bare strand, diam.	0.038 (inches)
Insulated strand, diam.	0.040 (inches)
Number of filaments	6328
Filament diameter	3.5 (microns)
Cu/S/C ratio	3.069
Packing factor	0.41
Conductor width	1.378 (in)
Conductor thickness	1.126 (in)
Conductor current density	50 (MA/m ²)
Overall coil current density	15.6 (MA/m ²)
Coil inductance	28 mH

Table 12. (con't)

Coil dimensions:

r_1	60
r_2	120
h	60
Total current	3 kA
Number of turns	58

The lattice braid is as shown in figure 33. This configuration is preferable to the cabled type conductors because of its superior cooling properties.

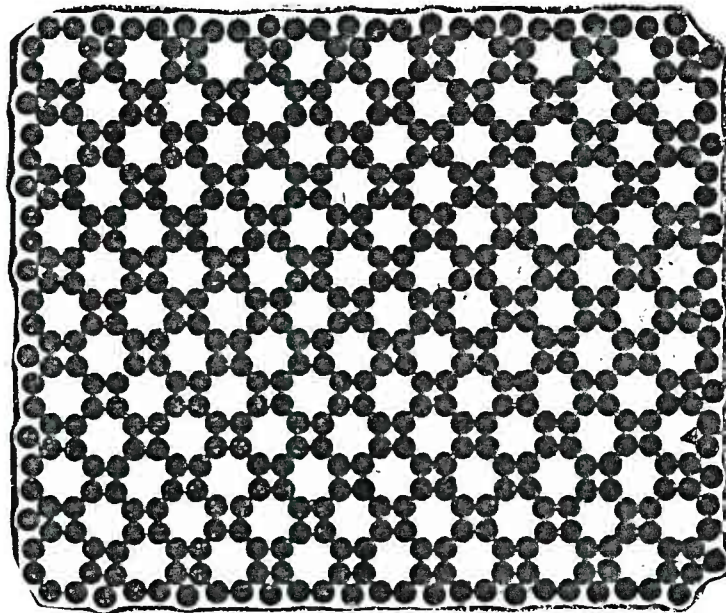


Figure 33. 503 strand lattice braid conductor.

Force-cooled conductors can be designed for a high recovery heat flux. The penalty one pays for the forced cooled conductors is the need for a pump to circulate the helium.

Coil Structure

It is advisable to consider a circular cross-section for the torus to minimize the mechanical stresses on the conductors specially when bent at the corners.

A simple calculation, which will require the same inductance, yields 80 turns. This means that the spacing will be $\frac{2\pi \times 60}{80} = 4.71$ cm.

The hoop stresses on the conductors tend to push them outwards. The configuration shown in figure 34 easily takes care of the forces in question.

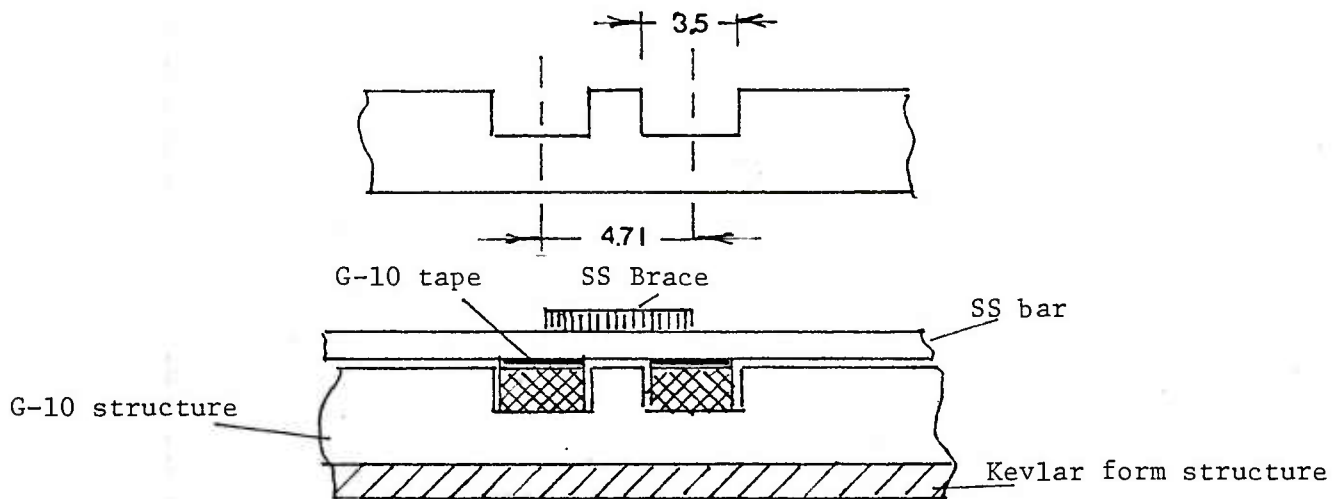


Fig. 34. Construction details for the winding support.

To reduce the thermal losses from the coil the torus is surrounded by a vacuum jacket. The use of superinsulation on the outer jacket is advised in order to avoid the use of a liquid nitrogen jacket (figure 35)

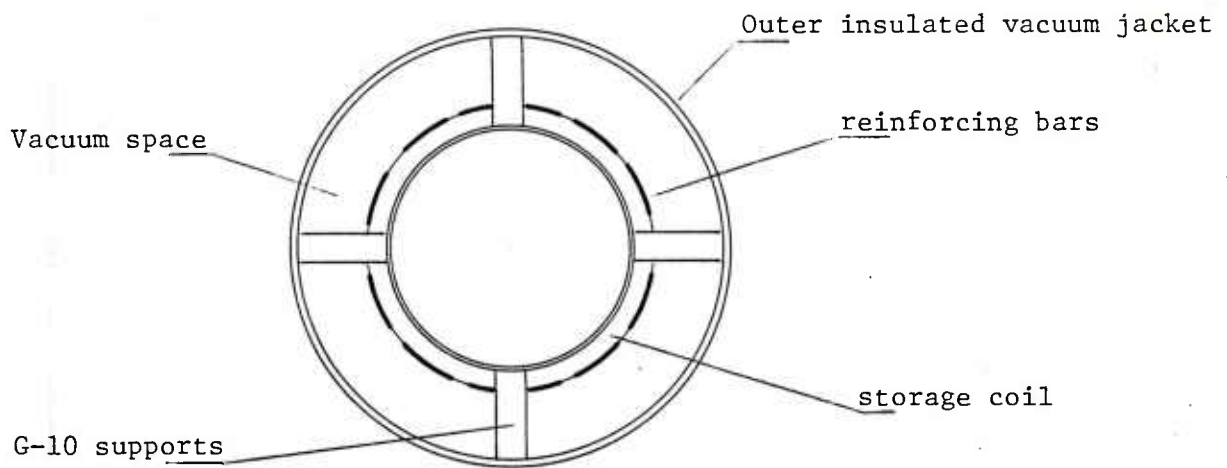


Figure 35. Cross section through storage coil.

Mass of Storage Coil

The mass of the storage coil is divided in unequal portions between

- a. The mass of the vacuum vessel
- b. The mass of the conductors and
- c. The mass of the reinforcing structures.

It turns out that the bulk of the mass is contributed by the reinforcing structures. These are the steel bars and their bracing straps. An upper bound for the mass needed can be had by means of the Theorem of the Virial (ref 42) which states

$$M = k \frac{E\rho}{\sigma_w} \quad (40)$$

where M is the mass of the structure, E the energy stored in the coil, ρ the specific density, k is a shape factor of the order of one and σ_w the maximum allowed working stress. For stainless steel which maintains its mechanical properties at cryogenic

temperature

$$\rho = 8 \text{ gm/cm}^3$$

$$\sigma_w = 1.1 \times 10^{10} \text{ dynes/cm}^2$$

$$\text{and } k = 1.1$$

Consequently for $E = 35 \text{ MJ}$; $M = 250 \text{ Kg}$.

Mass of Conductors

$$\text{Length of one turn} = 2\pi \times .30 = 1.885 \text{ m}$$

$$\begin{aligned} \text{Mass of one turn} &= 1.89 \times 10^2 \times 1.378 \times 1.126 \times 2.54^2 \times 8.9 \times 10^{-3} \\ &= 18.92 \text{ kg} \end{aligned}$$

$$\text{Mass for the whole coil} \quad 18.92 \times 58 = 983.83 \text{ kg}$$

Mass of Dewar

Construction of fiber glass (2 cm thick)

$$10^{-2} \times 1.885 \times 2\pi \times .9 = .1066 \text{ m}^3$$

$$\text{Mass } .1066 \times 2.8 \times 10^3 = 298.4 \text{ kg}$$

Total mass:

Conductors	933.83
Structure	250
Dewars	<u>298.4</u>
TOTAL	1482.23 kg.

Flux Pump

The source of current to the coil will be a flux pump of the rotating spot type. The overall characteristics of this pump can be inferred by means of some simple calculations based on the energy stored in the coil. It was found that with a current of 50×10^3 amps and an inductance of 28 mH, the energy stored in the magnetic field is 35 M joules. The chart (table 11) indicated that the charging time required was 30 secs.

We now select the following parameters for the pump

Number of poles 6

Field in Airgap 1.0T

Rate of rotation of 400 rps
field

To find the flux pumping rate, we start from the total flux linkage for the storage coil which is $(38 \text{ mH} \times 5 \times 10^4 \text{ amp}) = 1400 \text{ Web.}$

To reach this linkage in 30 seconds, the flux has to be pumped at the rate:

$$\frac{1400}{30} = 46.6 \text{ Webers/sec.}$$

If the area of one of the poles is A, then

$$46.6 = (6A) 1.0 \times 400$$

Hence, the area of each pole is 194.2 cm^2 . There is some benefit to space the "poles" of the pump by at least one width. This means that the moving "spots" will have dimensions which are roughly $(25 \times 7.77) \text{ cms.}$

The general configuration of a pump to meet the above requirements is shown in schematic form in figure 36.

The shape of the magnets shown in figure 36 indicate that "aa" must be greater than 7.76 to ensure adequate coverage of the superconducting foil. Suppose we make "as" 9.96, then the remaining dimensions are found from the requirements that the flux density in the web of width w cm does not exceed a value of 2.0T (typical for most steels) and the recess l will be able to accomodate the ampere turns needed to generate 1.0T in the air gap.

One derives w at once from:

$$\frac{(2\pi \times 60)w}{6} \times 2 \text{ (Tesla)} = (194) \times 1.0 \text{ (Tesla)}$$

which yields

$$w = 1.54 \text{ cms}$$

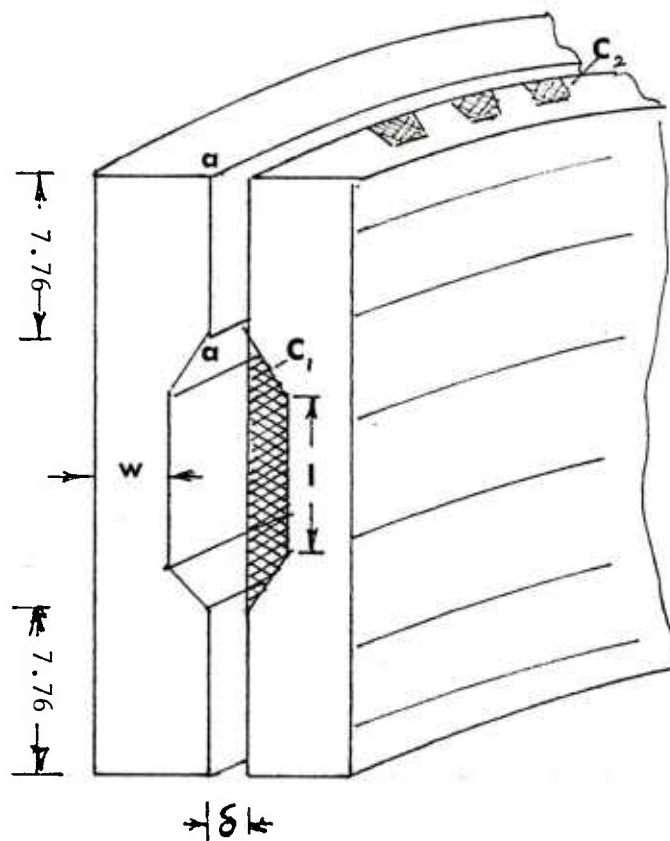


Figure 36. Configuration of flux pump magnets.

Choosing δ to be approximately 1 m/m, we estimate l from the number of amp-turns needed to establish 1T in the gap δ . This works out to be about 2000 amp-turns. Selecting a current of 10 amps, a recess of 3 m/m by 8 cm is quite adequate for the excitation coil.

To reduce the losses, we choose to have three sets of pumps operating in parallel. The arrangement is thus shown in schematic form in figure 37.

The weight of the armature is thus

$$28(2\pi \times 60 \times 2) \times 7.6 = 160 \text{ Kg/set}$$

Three sets represent 480 Kg.

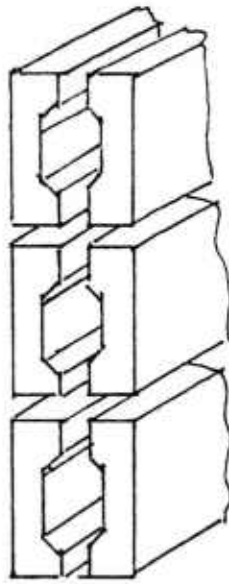


Figure 37. Method of compounding three flux pumps.

If we are less conservative we can use 1 set or perhaps two sets.

Now, it is to be remembered that the rotating field is provided by a distributed winding inserting in the pole pieces (fig. 38). Since it is required for the field to vary from a value below (or equal to) the critical field to a maximum, the d.c. bias will be only a fraction of the 1.0T.

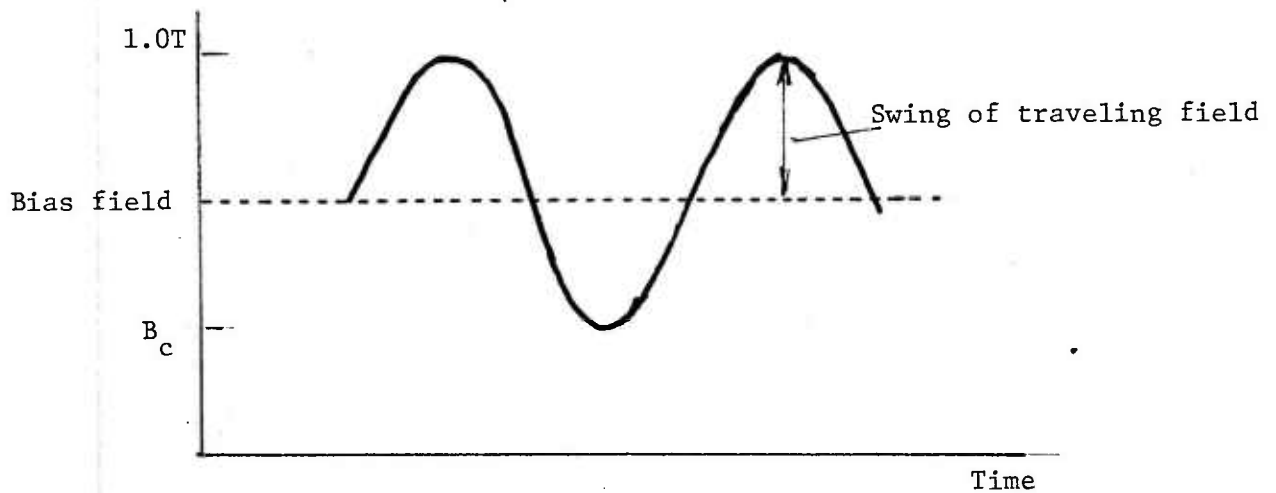


Figure 38. Temporal variation of the rotating magnetic field to actuate the flux pump.

To reduce the power to drive the travelling field, it is essential to have a fairly high value of B_c . By resorting to thin film, for Nb one can reach a value of $B_c \sim .6T$. The swing of the travelling field is thus of the order of $\pm 0.2T$ which is quite modest. The frequency, of course, is of the order of 400 cps.

The ampere turns required to provide the swing are approximately 200 amp turns. Here again, a current of 10 amps is very reasonable. Hence, we have 20 turns per coil. The slot has therefore 40 turns.

Driver Coils

It was found that the average velocity appears to increase linearly with the time (Eq. 20). This is consistent with the conservation of energy. Indeed, neglect-
in the losses

$$\begin{aligned} m \frac{dv}{dt} &= m \frac{dv}{dx} \frac{dx}{dt} = m \frac{d}{dx} \frac{v^2}{2} \\ &= I_r I_o \frac{\partial M}{\partial x} \end{aligned} \quad (41)$$

or

$$m \frac{v^2}{2} \bigg|_a^b = I_r I_o M \bigg|_a^b \quad (42)$$

Since the excitation pulses are applied twice per coil at the inlet and exit of the projectile from the driver coil, the kinetic energy increases in steps of $MI_o I_r$.

This is equivalent to

$$\overline{v^2} = k \overline{x} \quad (43)$$

or

$$\overline{v} = k_1 (\overline{x})^{1/2} \quad (44)$$

but

$$\overline{v} = \frac{d\overline{x}}{dt} \quad (45)$$

Therefore

$$\frac{d\bar{x}}{dt} = k_1 (\bar{x})^{1/2} \quad (46)$$

which yields

$$\frac{d\bar{x}}{\bar{x}^{1/2}} = k_1 dt \quad ; \quad d(\bar{x}^{1/2}) = \frac{k_1}{2} dt \quad (47)$$

$$\text{i.e. } \bar{x} = \left(\frac{k_1}{2}\right)^2 t^2 \quad (48)$$

$$\text{and } (\bar{v}) = \frac{k_1}{2} \sqrt{k} t \quad (49)$$

which checks our statement.

One can use these relations to find the design parameters for the gun.

Suppose we use n coils, then since there are two pulses per coil, we find that

$$m \frac{v}{2} f = 2 n M I_1 I_o \quad (50)$$

Consequently

$$M I_r I_o = \frac{mv_f^2}{4n} \quad (51)$$

In the above equation v_f is the final velocity at the muzzle of the gun. Now, fixing the current I_r to a constant value of 100 amps, we estimate the following options when we require $v_f = 1 \text{ km/sec}$.

$n = 5$

I_o (amps)	10^4	10^5	10^6
--------------	--------	--------	--------

M (H)	2.5	.25	.025
---------	-----	-----	------

$n = 10$

I_o (amps)	10^4	10^5	10^6
--------------	--------	--------	--------

M (H)	1.25	.125	.0125
---------	------	------	-------

Now the configuration of the two coils (driver and driven) is such that the coupling is very strong. Hence

$$M = \sqrt{L_{rr} L_o}$$

To get an idea for the size of L_o , we estimate the size of a cylinder of steel that will have a mass of 50 kg. Considering a length of 0.40m, we find that the radius is about 10.10 cm.

Since the velocity of the projectile is not constant with time, while the phase velocity on the transmission line is, one has to space the coils unequally. The synchronization is such that the energy is applied (in pulse form) only at the entrance of the coil.

To apply two pulses per coil, one must use a tapered line which can then have a velocity dependence duplicating that of the projectile. Under our simplified conditions

$$v_p = \frac{1}{\sqrt{LC}} = \text{phase velocity along the transmission line.} \quad (52)$$

The input impedance of the line is $Z = \sqrt{\frac{L}{C}}$. The energy input to the line, W_f is related to Z , through the relation

$$W_f = I_{rr}^2 Z \tau \quad (53)$$

where τ the interval denoting the temporal width $\tau \approx 10^{-4}$ sec. Combining the above equations one finds

$$L = \frac{W_r}{I_{rr}^2 \tau v_p} \quad (54)$$

Inspection of figure 40 allows one to take $v_p = 3.16 \times 10^3$ m/sec

Using $I_{rr} = 10^6$ amps, it is readily found that $L = 3.5$ mH

and $C = 28.6 \mu f$

If the inductance of the transmission line is taken to be that of L_{rr} , then one computes L_{oo} to be

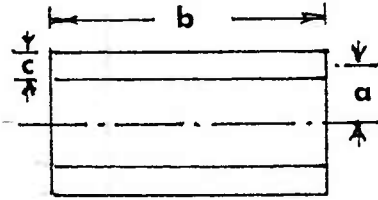
$$L_{oo} = \frac{M^2}{L_{rr}} = \frac{(0.0278)^2}{3.5 \times 10^{-3}} = 22.1 \text{ mH.} \quad (55)$$

Design of Driven Coil

The inductance of the solenoid is given by the formula (ref 43)

$$L = 0.019739 \left(\frac{2a}{b}\right) N^2 a K' \mu H \text{ (a cms)} \quad (56)$$

In our case the following conditions apply



$$\frac{2a}{b} = 1.0$$

$$K' = K - k$$

$$K = \text{Nagoaka factor} = 0.688$$

$$k = \text{fn}(c/2a) = 0.0316$$

$$K' = 0.656$$

Figure 39. Coil dimensions

Therefore, one finds for the number of turns $N = 414$ turns. Since the coil will be pulsed, one can increase the current density considerably beyond the value allowed for steady state. Indee, suppose we select a wire diameter of 2m/m, then the coil will consist of 4 layers with 100 turns per layer. The space factor is approximately 95%. The thickness of coil C works out to be 8 mm. while its length is 18 cm.

The coil characteristics are summared in the table below.

<u>Material</u>	<u>Copper</u>	<u>Aluminum</u>
Mass (kg)	31.1	8.39
Resistance (ohm)	1.78	4.43
Temperature rise ($^{\circ}\text{C}$)	1.58×10^{-3}	3.15×10^{-2}
Cooling Load		

The main contributors to the heat losses in the pulsed power system are the switch, the storage coil and the flux pump. The characteristics of these components have already been discussed in previous sections. We will concentrate here in estimating the heat dissipation in the individual components to estimate the cooling

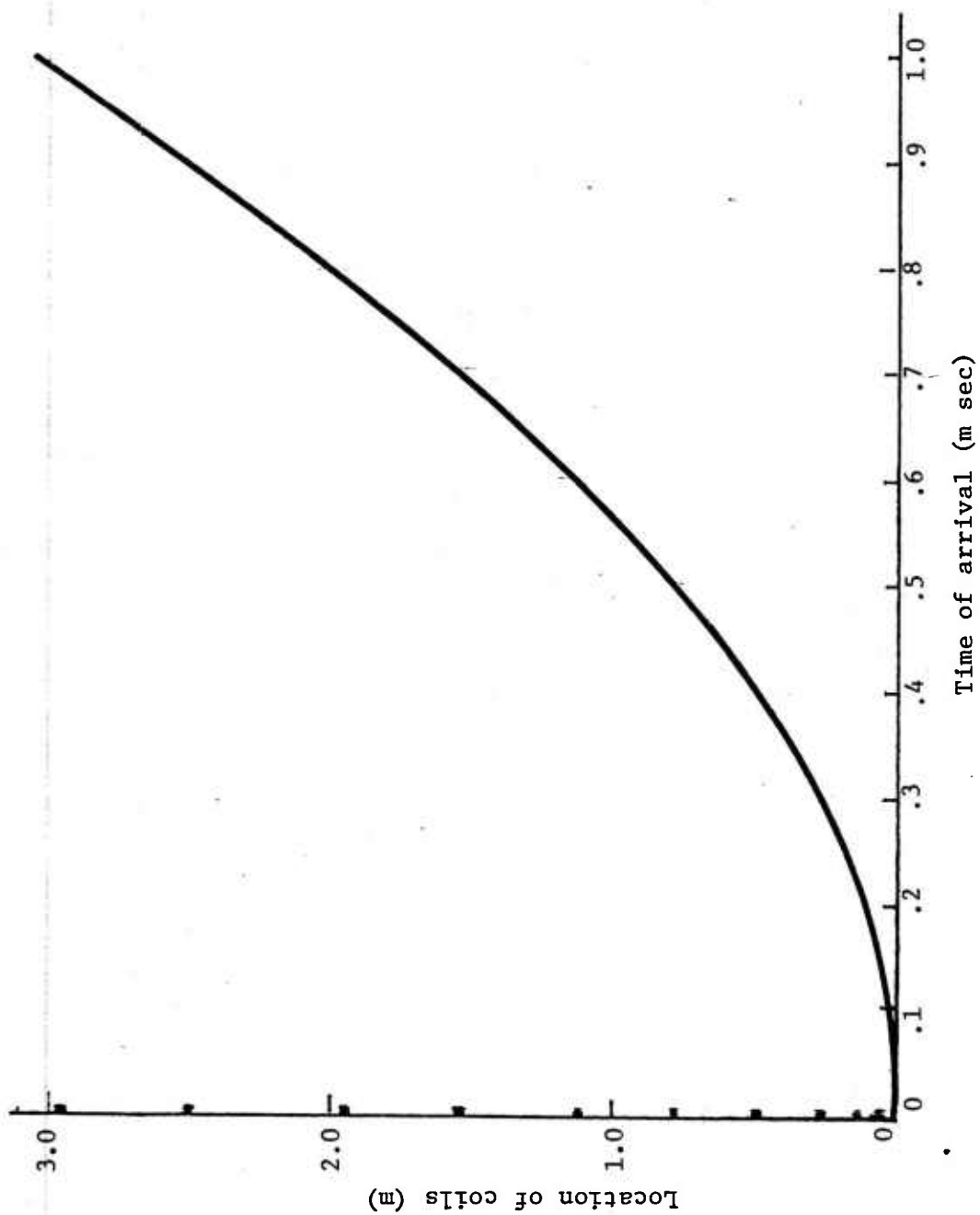


Figure 40. Location of the coils for equal intervals for the transmit time of the projectile.

load required.

Heat Losses from Switch

For a storage system of 30 MJ and for an initial current of 50 k amps in the superconducting storage inductor, the voltage developed is expected to be 300 kV on the assumption that the energy is delivered in 2 msec.

Using the same concept as discussed elsewhere (ref 44), fifteen switches each with a hold-off capacity of 20 kV should be able to interrupt the required current. Each one of the switches is expected to have a time constant of a microsecond (a conservative estimate). Consequently, the heat losses from the switches will be $(50 \times 10^3 \times 300 \times 10^3) \times 10^{-6}$. This is estimated to be 15 kJoules.

Although the switch losses are large, they actually represent a small fraction ($7.5 \times 10^{-4}\%$) of the energy stored. The twenty switches are proposed to be immersed in a helium container as discussed in reference 44. The advantage of the design of reference 44 is that the mass of the copper used in the construction of the switch is large enough that the temperature rise can be extremely low thus economizing on the amount of helium evaporated.

Heat Losses from Storage Coil

The steady heat losses from the toroidal storage coil discussed in Storage Coil section, is fairly small. By resorting to superinsulation, it is readily found that with an insulation blanket 5 cm thick the losses can be kept below the value of 7.5 watts.

Heat Losses from Pump

Of the several types of flux pumps available, the rotating spot flux pump (ref 45) is the most appropriate to the present system because of the very high efficiency that can be reached (99.95%) and because of the flexibility of the pump which permits the use of a rotating field to eliminate the mechanical rotation of the pump.

In spite of the high efficiency, the losses are substantial in terms of the helium required to compensate for the losses. Specifically, to store 30 MJ, one finds that the energy dissipated in the pump is 150 watts. Since these losses are accounted for by eddy current dissipation in the normal spots of the flux pump, the losses occur on a steady state basis.

Capacity of Cooling Plant

The crucial issue in the cooling of the system is not the total loss incurred, but the repetition rate of the gun which defines the rate of cooling energy required to make up for the losses.

Combining all the losses discussed so far it appears that the losses amount to about $1.3 \times 10^{-3}\%$ of 30 MJ or 39 kJoules. If one allows a charging time of 30 sec, then the plant capacity is 1.3 kWatts. According to the discussion of Section 2.2 this would call for a power plant of .52 MW to actuate the liquifiers.

Summary and Conclusions for Reference Design I

The design discussed in details in the previous sections has a number of features that are very attractive from an operational point of view. To fix the ideas, these are summarized below.

Advantages

1. The driven coil of the accelerator is excited through brushes. By maintaining the current in the coil to a low value, the problem of wear at the brushes is minimized thus increasing the reliability of the system.
2. The driver coils carry large currents - of the order of a megamp. These coils are pulsed in sequence effectively increasing the specific repulsion force produced by the coils. This is because this force which is proportional to $\frac{dM}{dx}$ is one order of magnitude greater than the specific force found in

a rail gun. In the latter case, the force goes roughly like $\frac{dL}{dx}$.

3. The arrangement proposed in Reference Design I eliminates the use of switches, the pulsing sequence relying on the delay time of the transmission line to provide the correct timing of the excitation current.
4. The use of pulses minimizes the losses in the gun and leads to an optimization of material use.
5. The combination of a superconducting power source and a launcher constructed of normal material has the beneficial effect of improving the efficiency of the system from the point of view of energy consumption and weight.
6. The use of a travelling pulse has the unusual property in that the magnetic field is concentrated at the spot where the acceleration is taking place, hence no unused energy is left in the launcher after the projectile has been ejected.

Disadvantages

Two undesirable features of the Reference Design I are the appearance of very high voltages at the breech of the gun and the need for a time reversal of the excitation current for the driven coil.

Although the high voltage can be used with the proper use of insulation, it is advisable to redesign the system so as to maintain the voltage within the bounds of a safe lower voltage. The use of an alternating excitation current for the driven coil is not recommended since it, too, could lead to a very high voltage on the driven coil which cannot be easily taken care of.

In view of the above objections, the second design was initiated with the purpose of maintaining the desired features outlined above and at the same time altering the concept to eliminate the unwanted features.

The chief characteristics of the first design are:

Mass of projectile	50 kg
Terminal velocity	3 km/sec
Length of launcher	6 m
Energy used (for acceleration)	25 MJ
Mass of coil	8.39 (kg)
Energy for cooling	0.52 MW
Charging time	30 sec.

Outline of Reference Design II (RD II)

Basic Concept

The operational theory of Reference Design II resembles in many ways that of the previous design. There are, however, some fundamental differences. To fix the ideas, the electromagnetic gun is shown in in schematic form in figure 41.

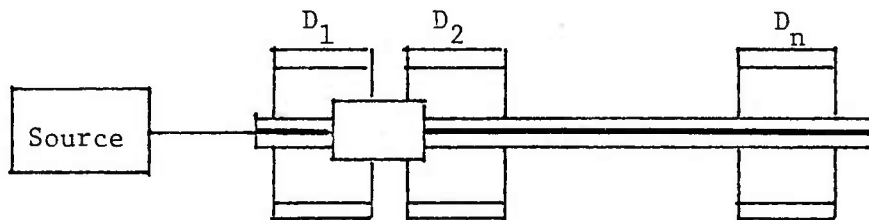


Figure 41. Schematic of gun used in RD II.

The driven coil C is excited with direct current from an independent source - just as in RD I the current in C is kept at a low enough value that the wear at the brushes is minimal.

The current in the driver coils D is large, pulsed, and is channeled to the coils D through a transmission line. The currents in the D_1 , D_2 , ... reversing to exert a force on C as it enters the D coils as well as it emerges.

As the coil accelerates, the transit time through the coil becomes shorter. Accordingly, the effective frequency of the currents in D_2 increase. But the voltage across the driver coils D_1, \dots is mostly contributed by the reactive voltage drop $L_n \frac{dI_n}{dt}$ where L_n is the self inductance of the D_n coils while I_n is the current in the same coil.

But it is clear that

$$L_n \frac{dI_n}{dt} \approx L_n \frac{I_n v}{b} \quad (57)$$

where v is the velocity of the C coil and b is its length. The various coils D_1, \dots therefore, must be so designed as to optimize the electromagnetic repulsion force and at the same time keep the voltage within bounds.

Now the force between the coils C and D depend not only on the current in these coils, but also on the relative dimensions of these coils. From classical electromagnetic theory and as mentioned previously under Interior Ballistics of Gun, the force is proportional to $\frac{dM}{dx}$. The gradient of the mutual, however, is a function of four geometric parameters corresponding to the radii and lengths of the coil. It can be shown that these four parameters can be reduced from four to two as discussed in the attached paper (Appendix A). In the same paper, there is a discussion on the optimization procedure used to locate the maximum-maximum of $\frac{dM}{dx}$.

The design of the coils subject to the requirement of optimum force and ascribed maximum voltage requires a laborious procedure involving the solution of simultaneous differential equations.

Accordingly, an algorithm was developed (Appendix B) which describes the procedure to numerically program on a computer the solution of these equations.

The result of these calculations has been included in the paper of Appendix A.

Since there are several similarities between the components used in the two designs the details for the calculations will be omitted.

Construction Features of Gun

Figure 42 shows the design features of the gun, while figure 43 shows the constructional details of the pulsed power source. Figure 44 shows the suggested shape of the transformer needed to produce the current sign reversal.

The main design parameters are tabulated below.

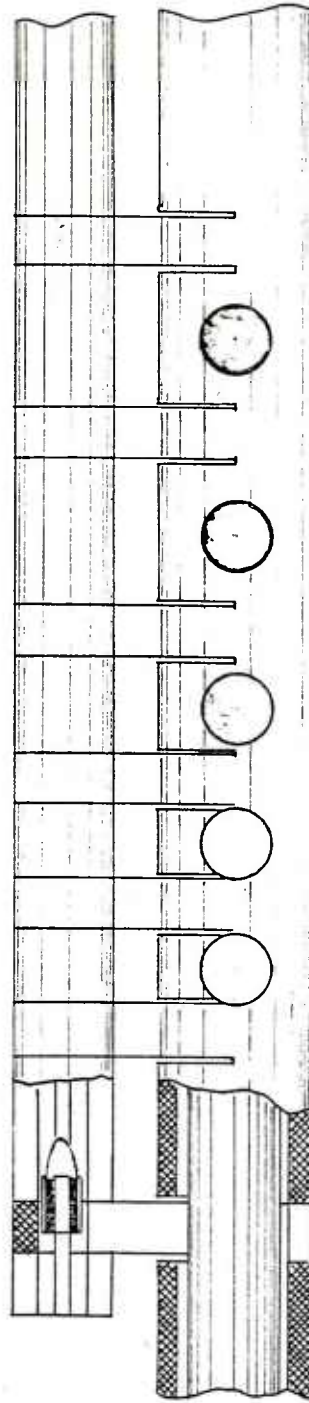
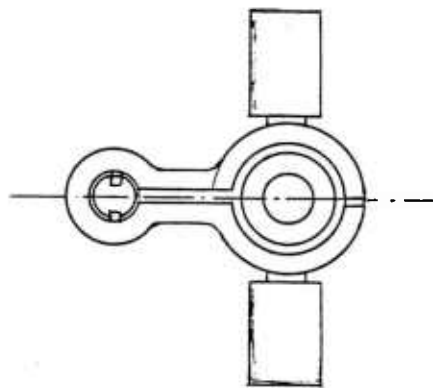
Mass of projectile	50 kg
Exit velocity	1 km/sec
Energy of projectile	25 MJ
Conductor mass	20.27 kg
Length of gun	3 m
Number of driver coils	10
Inductance of driven coil	129.2 mH
Mutual inductance	12.5 mH
Inductance of driver coil	1.2 mH

CONCLUSIONS

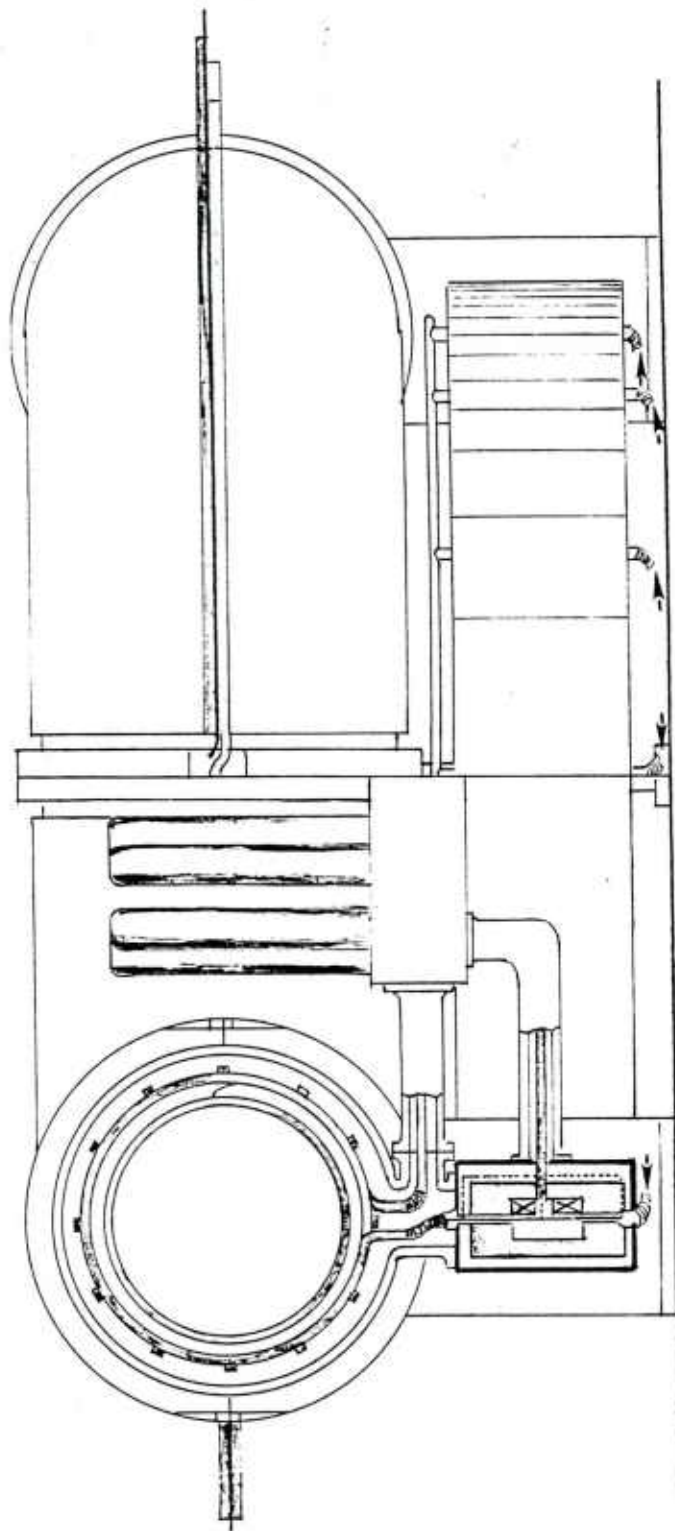
The concluding remarks are divided into two parts. The first part deals with the assessment of the superconducting technology while the second is concerned with innovations and improvements in the design and construction of electromagnetic guns.

Superconducting Components

The survey of the state-of-the-art of applied superconductivity has shown quite clearly that commercially available superconductors operate with current densities that are two order of magnitudes higher than conductors constructed out of normal materials even when these conductors are cryogenically cooled. Furthermore, the success of the technology of internally cooled superconductors leads to a substantial savings in weight and simplicity of construction of the thermal insulation. In addition, it eliminates the need for bulky cryostats.



Scale 0 1m

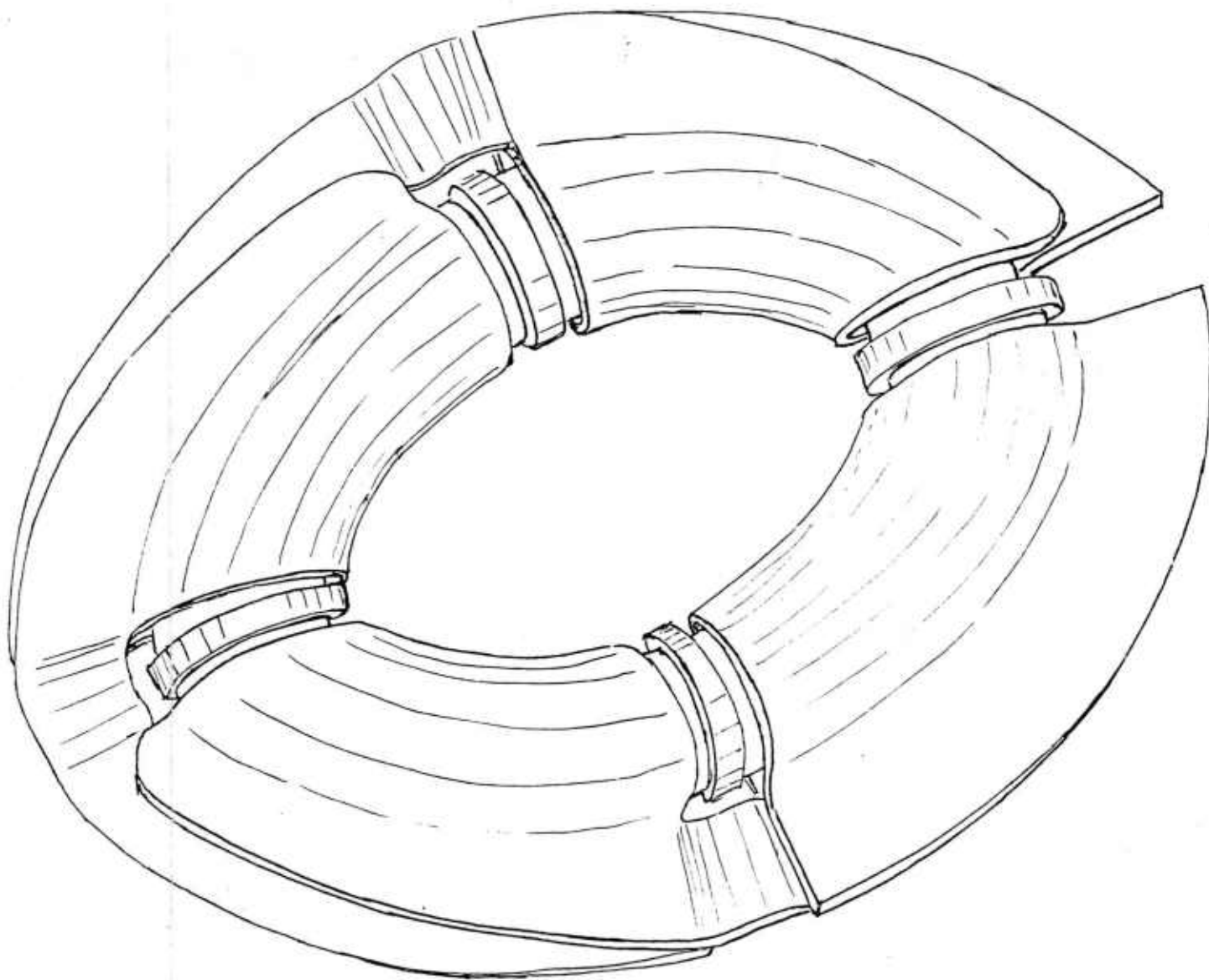


Scale 0 0.5m

collaborative planners, Inc.

Fig. 43

Pulsed Source



collaborative planners, inc.	Fig. 4 4
------------------------------	----------

Transformer

Improvements in the technology of constructing flux pumps have led to the ability of charging superconducting inductors at the very high rates. This feature of flux pumps is most attractive to repetitively fired electromagnetic guns.

Through the use of thin films, superconducting switches of very large current capacities, can be constructed. By proper design of the thermal cooling of superconducting switches, repetitively operated opening switches of very long life can be constructed.

The ability to use superconductors at extremely high magnetic fields opens up the possibility of constructing inductive storage systems with very high energy densities. When pulsed energy sources are considered inductive energy sources for energy levels and time constants applicable to electromagnetic guns are by far superior to all the other sources presently used.

The size and efficiency of the helium liquifiers is improving steadily. The present state-of-the-art indicates that 1W of cooling at liquid helium temperatures requires a 400W capacity for the liquifier. Since a well-designed system will rarely exceed 1.5kW of cooling for the largest gun required, the overall weight of the cooling plant will always be a small fraction of the total system.

The general conclusion is that a superconducting pulsed source is an efficient, compact and highly reliable source which should be considered seriously for heavy, land based guns.

Improvements in Gun Design

The two designs studied have demonstrated that it is possible to construct an electromagnetic gun with the following attractive features.

1. Switchless design - The introduction of the delay line permits the excitation of the driver coils in sequence thus completely eliminating the need for switches to divert the current to the coils.

2. High efficiency - The transfer of energy from a pulsed source [irrespective to its nature homopolar or inductive storage] to the transmission line assures a very high efficiency process because the source effectively "looks" a pure resistance viz., the characteristic impedance of the line.

3. Brush wear - By reducing the current in the driven coil to a low value of 100 amps the concern of erosion at the brushes is considerably reduced. Even at high velocities the contact resistance at the brushes should be reasonably maintained and the problem of arcing minimized because of the low current densities.

4. Force optimization - The detailed analysis and numerical program which have been developed makes it possible to optimize the force exerted on the driven coil (projectile). The ultimate result is an increase in the ratio of pay load to weight of the driven coil.

In conclusion, the synchronous coaxial gun developed in the study is a simple, reliable device of high efficiency, and low weight and which has furthermore, the great advantage of great mechanical strength (because of axial symmetry) and does not require switches for its operation.

REFERENCES

1. D. Shoenberg, "Superconductivity" (Cambridge University Press, 1952)
2. J.E.C. Williams, "Superconductivity and Its Applications" (Pion Ltd., London 1970)
3. A.A. Abrikosov Sov. Phys. J.E.T.P. 5, 1174 (1957)
4. W. DeSorbo Proc. Seventh Int. Conf. on Low Temp. Phy. (Toronto Univ. Press 1961)p.370
5. Yetter et al., Phil. Mag. B46, 523 (1982)
6. J. Muller Rep. Prog. Phys. 43, 641 (1980)
7. H. Hartman et al., Z. Anorg. Chem, 198, 116 (1931)
8. G.F. Hardy et al., Phys. Rev. 87, 884 (1953)
9. B.T. Matthias et al., Phys. Rev. 95, 1434 (1954)
10. D. Dew-Hughes Cryogenics 15, 435 (1975)
11. J.D. Verhoeven et al., Appl. Phys. Lett. 33, 101 (1978)
12. R. Roberge et al., Appl. Phys. Lett. 34, 111 (1979)
13. C.G. Homan et al., Phys. Letters 87 A, 57 (1981)
14. F.C. Maticcotta et al., IEEE Trans. on Mag. MAG-19, 897 (1983)
15. Z.J.J. Stekley Jour. Appl. Phys. 37, 324 (1966); 42, 65 (1971)
16. C.R. Spencer et al., IEEE Trans. on Mag. MAG 15, 76 (1979)
17. K. Tachikawa Adv. Cryog. Eng. 28, 34 (1981)
18. Ref. (16)
19. W.Y. Chen IEEE Trans. on Mag. MAG-19, 328 (1983)
20. A.G. Montgomery et al., IEEE Trans. on Mag MAG-15, 794 (1979)
21. M.O. Hoenig Cryogenics 20, 373 (1980)
22. M.O. Hoenig Cryogenics 20, 427 (1980)
23. M. Sittig "Cryogenics and Its Applications" (D. van Nostrand & Co. NY 1963)
24. M. Knudsen "The Kinetic Theory of Gases" J. Wiley & Sons, NY (1952)
25. "Experimental Cryophysics" Ed. F.E. Hoare et al., (Butterworth, London 1961)
26. R. Barron "Cryogenics Systems" (McGraw Hill, NY 1966)
27. T.R. Strobridge et al., Adv. Cryog. Eng. 12 576 (1966)
28. F.W. Pirtle et al., Adv. Cryog. Eng. 27, 501 (1982)
29. Koch Products Catalog, Framingham, Massachusetts
30. F. Irie et al., IEEE Trans. on Mag. MAG-19, 672 (1983)
31. R. Carruthers "High Magnetic Fields" (John Wiley NY 1962) p.307.

References, con't

32. Ref. (31)
33. S.L. Wipf NASA Tech. Transl. F-15109, Rep. N73-31676 (1973)
34. P. Komarek et al., Proceedings of International Conf. on Magnet Technology Rome, p. 313 (1975)
35. O.K. Mawardi, IEEE Trans. on Magnetism MAG 18, 60 (1982)
36. G. Campbell et al., "Fourier Integrals" (Van Nostrand Co., NY 1962)
37. H.B. Brooks J. Res. Nat. Bur. Stand. 1, 289 (1931)
38. G.P. Harnwell "Principles of Electricity and Magnetism" (McGraw Hill, NY 1939)
39. W.V. Hassenzahl et al., LASL Tech. Rep. LAUR-73-73 (1973)
40. F.W. Grover, "Formulas for Mutual and Self Inductances" (Dover Publications NY 1962)
41. M. Morpugo in "Particle Accelerators" (Gordon and Breach Science Publishers, Ltd) Vol. I, 1970; M.O. Hoenig in Ref. (21) and Westinghouse Electric Co. Tech. Rep. submitted to Los Alamos Sci. Lab. #L-48-8407C-1, (1978)
42. O.K. Mawardi, LASL Tech Rep. LA-55953-MS (1975)
43. Ref (40)
44. O.K. Mawardi, et al., IEEE Trans. on Mag. MAG-19, 1067 (1983)
45. O.K. Mawardi, et al., IEEE Trans. on Mag. MAG-15, 28 (1979)

APPENDIX A

DESIGN DETAILS FOR REFERENCE DESIGN II

O. K. Mawardi
Collaborative Planners, Inc.
Cleveland, Ohio 44106

ABSTRACT

A new concept for a coaxial accelerator is described. The scheme is a hybrid combination of a travelling wave accelerator and of a distributed impulse driver. The main current to the launcher is delivered at one end of a transmission line and is periodically diverted to driver coils. The current to the driven coil, on the other hand, is delivered from an independent source through rails. With this system no switches to modulate the current to the driver coils are needed. The paper presents details of the system components used and of the predicted performance of the launcher.

I. INTRODUCTION

An extensive amount of work on coaxial accelerators is presently reported in the literature⁽¹⁾. These launchers have the great advantage over rail guns accelerators in that the current in the moving coil can be kept at a relatively low value⁽²⁾ thus minimizing arcing and erosion at the brushes. The current in the stationary coil, however, is much larger since the force on the moving coil is proportional to the product of the two currents.

Now, in a coil driven accelerator the current in the stationary coils has to be reversed periodically⁽³⁾ as the moving coil enters and exits the fixed coil. The required temporal behavior of the current to the stationary coils is obtained by modulating with switches the output from a d.c. source⁽⁴⁾.

As the exit velocity of the projectile from the launcher reaches speeds of 1 km/sec or higher, the switches must respond in less than 10^{-4} sec. Available switches today are unable to meet these requirements of repetitive switching times and large current ratings.

The present paper is concerned with the description of a novel scheme that avoids the use of the higher current, fast switches needed for the launchers. The first part of the paper contains a discussion of the optimization of the force on the driven coil. This is followed by a description of the proposed concept. The remaining part of the paper is devoted to design considerations.

II. FORCE OPTIMIZATION

According to the classical electromagnetic theory, the force between two coaxial cylindrical coils (Fig.1) C_1 and C_2 in which circulates I_1 and I_2 respectively is given by the expression

$$F = I_1 I_2 \frac{\partial M}{\partial s} \quad (1)$$

In the above equation, M stands for the mutual inductance between the two coils and s is the relative distance between them. $\frac{\partial M}{\partial s}$ changes signs as the coil C_1 moves from the left of C_2 to its right i.e. as s goes from a negative to a positive value. It is apparent, therefore, in order for the direction of the force to remain unaltered for constant I_1 , that I_2 has to change signs with $\frac{\partial M}{\partial s}$.

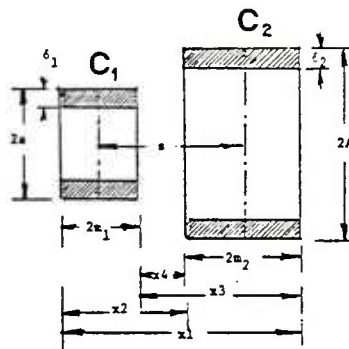


Fig. 1 - Notation Used in Text

The mutual inductance M is explicitly given by

$$M = 0.002 \frac{\pi^2}{4m_1} a^2 N_1 N_2 f \times 10^{-6} \text{ Henrys} \quad (2)$$

where N_1 , N_2 are the number of turns of C_1 and C_2 and f is a function which has been evaluated by Grover⁽⁵⁾. The function f depends on x_1 , x_2 , x_3 , x_4 , s , m_1 , m_2 , a and A . The definition of these variables is found by inspection of Fig. 1.

For any one set of variables m_1 , m_2 , a and A , there is a value of s at which $\frac{\partial M}{\partial s}$ (or $\partial f / \partial s$) reaches a maximum. Introducing the dimensionless quantities $s/m_2 = \zeta$, $m_1/m_2 = \xi$, $A/m_2 = \beta$ it is more convenient to investigate $\partial f / \partial \zeta$ rather than $\partial f / \partial s$. We now search for $\partial f / \partial \zeta$ max for a fixed ξ, β , evaluate this maximum, and plot the value of these maxima as a function of ξ and β (Fig. 2). This figure shows that there is a pronounced maximum - for any ξ at a value of $\beta \approx 1$. There is an advantage, therefore, to operate the accelerator in the vicinity of these maxima-maxima.

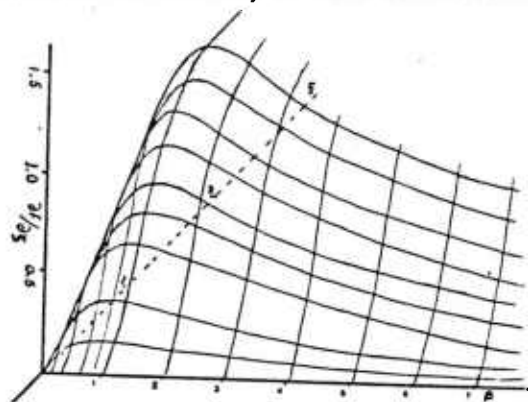


Fig. 2 - Three Dimensional Plot of the $\partial f / \partial \zeta$ Function for the Variables ξ and β . Notice that the Curve $\beta = 1$ Reaches a Plateau.

III. DESCRIPTION OF ACCELERATOR

The main features of the accelerator is summarized in schematic form in Fig. 3. The proposed accelerator consists of a repulsion coil arrangement in which the moving coil C is guided by rails. The rails also serve as bus bars through which a current can be fed to the coil C . The moving element C is excited from

*Supported in part by ARRADCOM

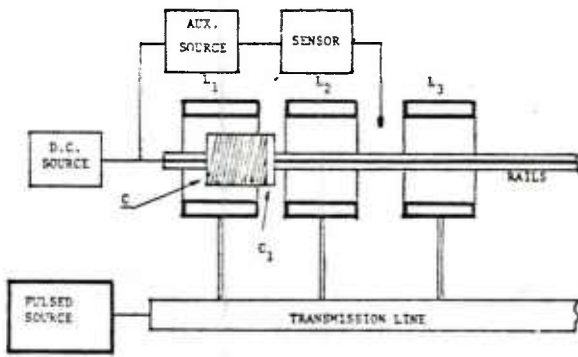


Fig. 3 - Schematic of Accelerator System

a d.c. source. Another coil C_1 wound on the same former of C is connected to a low power pulsed source. The function of C_1 will be discussed below. The main pulsed energy source is connected to a transmission line. The driving coils L_1, L_2, \dots are attached at period intervals of the line. When a pulse is initiated at one end of the transmission line, this pulse will propagate down the line and reach the driver coils in succession. These coils can thus be excited sequentially without resorting to any switching device.

It is essential to design the transmission line so that the main pulse from S travels down the line in synchronism with the coil C . The design procedure outlined below will yield a speed of C approximately equal to that of the pulse. Fine adjustment for synchronism is secured through the coil C_1 . This coil is excited with pulses initiated by commands from sensors detecting the position of the driven coil and initiating small acceleration or deceleration corrections to maintain synchronism.

IV. DESIGN PROCEDURE

The derivation of the dynamics of the projectile in the accelerator is found by means of piece-wise solutions. Each one of these solutions will treat the passage of the projectile into one coil. The general solution for the behavior of the projectile throughout the gun is then constructed by piecing together elementary solutions through a match at the exit of one coil and inlet at the neighboring coil.

Let us consider the r th coil L_r in which circulates a current I_r . If we denote by s the displacement of the projectile inside L_r , then the force equation requires that

$$m \frac{dv}{dt} + \alpha v = I_r I_o \frac{\partial L_{ro}}{\partial s} \quad (3)$$

In the above, m is the mass of the projectile, v its velocity, I_o is the d.c. current in the coil C , L_{ro} is the mutual inductance between L_r and C and α is a coefficient to account for the mechanical friction losses.

A second relation for the motion of the projectile is found from the circuit equivalent, that describes the back e.m.f. as a result of the motion. This equation is

$$L_{rr} \frac{dI_r}{dt} + v I_o \frac{\partial L_{ro}}{\partial s} + R_{rr} I_r = E_r(t) \quad (4)$$

The symbol L_{rr} stands for the self inductance of the r th coil, R_{rr} for its resistance and E_r is the voltage appearing across the r th coil.

Now, it was mentioned in Section II, that the

maximum value of $\frac{\partial L_{ro}}{\partial s}$ (called $\frac{\partial M}{\partial s}$ in that section) depended on the geometry of the two interacting coils. In fact, we indicated that the force was a maximum for $\xi = 1 = \beta$. Furthermore, it is known that a coil with a Brooks' configuration⁽⁶⁾ has the minimum mass for a given inductance. These criteria fix the proportions for the two coils and allow one to calculate the inductances.

By eliminating the current I_r between Eqs. (3) and (4) we find

$$\frac{d^2 v}{dt^2} + \left(\frac{\alpha}{m} + \frac{R_{rr}}{L_{rr}} \right) \frac{dv}{dt} + \left(\frac{\alpha}{m} \frac{R_{rr}}{L_{rr}} + \frac{1}{m L_{rr}} \left(I_o \frac{\partial L_{ro}}{\partial s} \right)^2 \right) v = \frac{I_o}{m L_{rr}} \left(\frac{\partial L_{ro}}{\partial s} \right) E_r \quad (5)$$

On the basis of the discussion in Section II, we know that $\frac{\partial L_{ro}}{\partial s}$ is a function of position. Its functional dependence, however, is such that we can replace $\frac{\partial L_{ro}}{\partial s}$ by a pulse-like function. This means that

one imagines the repulsive force between the coils to take place mainly as the driven coil enters and exits the L_r coils. With this approximation, Eq. (5) is

solved at once to yield

$$v_r(t) + \frac{1}{\sqrt{2\pi}} \int_{-\infty}^{\infty} \frac{\tilde{E}_r(\omega) e^{i\omega t} a d\omega}{(m L_{rr} a^2 + \frac{\alpha}{m} \frac{R_{rr}}{L_{rr}} - \omega^2 + i\omega \left(\frac{\alpha}{m} + \frac{R_{rr}}{L_{rr}} \right))} \quad (6)$$

The symbol $\tilde{E}_r(\omega)$ stands for the Fourier transform of the voltage applied to the L_r coil and $a = \frac{I_o}{m L_{rr}} \left(\frac{\partial L_{ro}}{\partial s} \right)_{\max}$.

Since the voltage excitation is in the form of two pulses, one positive at the entrance to L_r and a negative at the exit, and of magnitude E_r , we find for the value of the velocity between $s = 0$ and $s = m_1$

$$v(t) = \frac{1}{\sqrt{2\pi}} E_r \exp\left(-\left(\frac{\alpha}{m} + \frac{R_{rr}}{L_{rr}}\right) \frac{t}{2}\right) \frac{\sin(a\sqrt{m L_{rr}} t)}{\sqrt{m L_{rr}}} \quad (7)$$

Since $a\sqrt{m L_{rr}} \ll 1$, the above simplifies to

$$v(t) = \frac{E_r}{\sqrt{2\pi}} \text{ at } \quad (8)$$

when all losses are neglected. This idealized solution yields for the location of the projectile

$$s = \int v dt = \frac{E_o}{\sqrt{2\pi}} \frac{at^2}{2} \quad (9)$$

or

$$v = \left(\frac{E_r}{\sqrt{2\pi}} \right)^{1/2} S \quad (10)$$

The approximate relation (10) is a key relation in that it yields the length of the accelerator (or which is equivalent the number of driver coils) needed to achieve an exit velocity for a given voltage E_o and excitation current to the driven coil. The same relation determines the arrangement of the driver coils to achieve synchronization. Fig. 4 shows the dependence of the location of the projectile on the time.

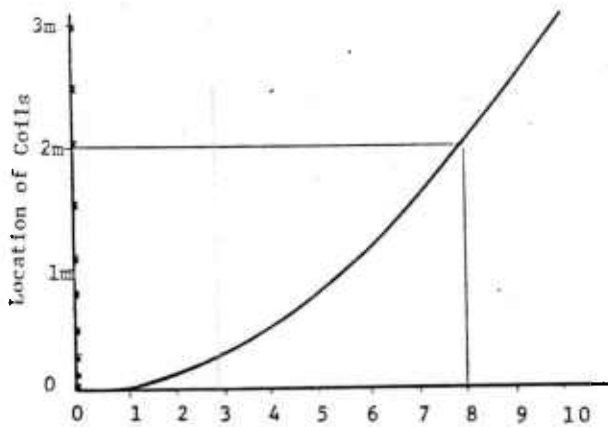


Fig. 4 - Procedure Used to Find the Location of Driver Coils by Means of Eq.(9)

Let us imagine the driver coils to be connected at equal distances along the transmission lines. Therefore, the non dispersive behavior of the lines will cause current pulses to occur at equal intervals of time. In order for the pulse to be in synchronism with the projectile, the coils have to be spaced to satisfy the quadratic law.

V. CHARACTERISTICS OF TRANSMISSION LINE

One of the simplest designs for the transmission line is to use a ladder of low pass filters. The number of quadrupoles in the ladder is taken to be equal to the number of driver coils. Fig. 5 shows one of these quadrupoles.

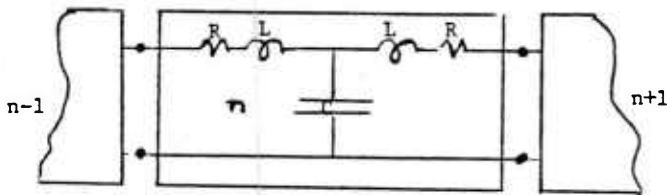


Fig. 5 - Typical Ladder in the Chain

The values of the inductance L and of the capacitance C are found from

$$v_o = \frac{2}{\sqrt{LC}} \quad (11)$$

where v_o is the velocity of propagation of the pulse

$$\sqrt{\frac{L}{C}} = R_o \quad (12)$$

in which R_o is the characteristic impedance of the transmission line. R_o is selected such that it is equal to the internal impedance of the pulse source thus assuring effective energy transfer. The dissipative element in the quadrupole of Fig. 5 represents the ohmic losses in the coil.

An efficient way for the transfer of energy to the driver coils consists in incorporating the inductance of the driver coil in L . Clearly one selects L large enough that the inductance L_r is smaller than that of L .

Because of the losses in the line the pulse will broaden as it travels down. The shape of the pulse can be shown⁽⁷⁾ to be expressed by

$$I_n = \frac{d}{dt} \left(\frac{2E_o}{L} e^{-R/Lt} J_{2n}(v_o t) \right) \quad (13)$$

where n locates the position of the n^{th} quadrupole E_o is the applied voltage at the beginning of the line and J_{2n} is the Bessel function of the first kind.

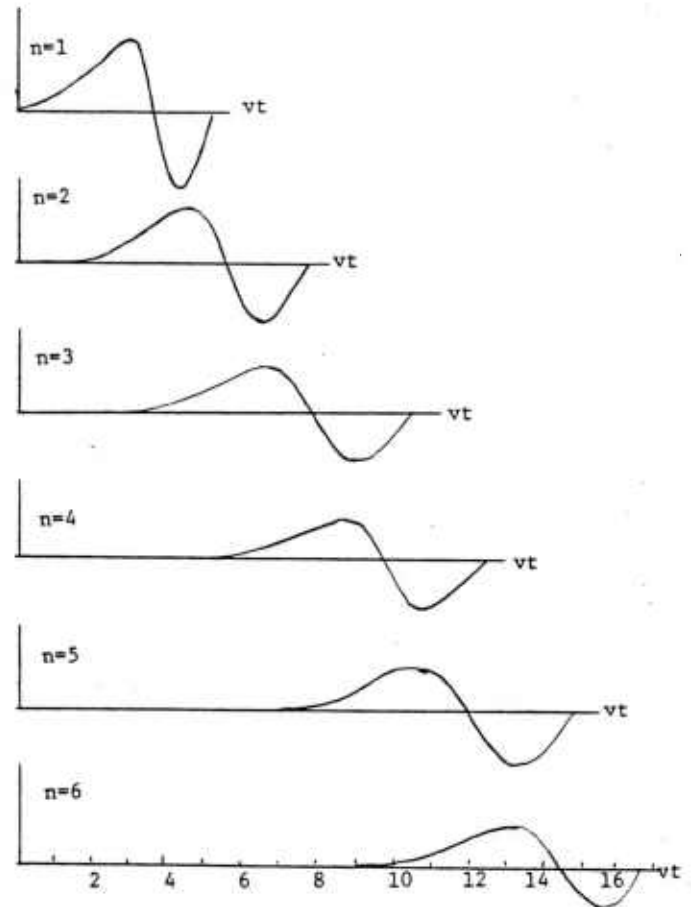


Fig. 6 - Temporal Behavior of the Current in the First 6 Driver Coils of an Accelerator Consisting of 10 coils.

The temporal behavior for the propagation pulse is shown in graphical form in Fig. 6. The calculations were made for the case of wave propagation speed of 1 km/sec and for a chain of 10 coils. Fig. 6 shows the temporal behavior of the current in the first 6 coils.

An important aspect of the design is to use a high enough value of the source that the initial acceleration is large enough to allow the projectile to reach the final velocity in the prescribed length of the accelerator which is taken as 3m.

The design parameters of the gun thus turn out to be

$$E_o = 100 \text{ KV}$$

$$\text{Number of turns in } L_r = 25$$

$$\text{Number of turns in } C_o = 1000$$

$$\text{Current in } C_o = 100 \text{ amps.}$$

$$\text{Mutual inductance} = 1.25 \text{ mH}$$

$$\text{Length of accelerator} = 3 \text{ m}$$

$$\text{Final velocity} = 1 \text{ km/sec}$$

REFERENCES

- 1) See for instance, Electromagnetic Launch Review, Sept. 1982 (DARPA), Washington, D.C., also H. Kolm, Proc. Third Symp. on Space Manuf., 1977 (AIAA)
- 2) O. K. Mawardi, IEEE Trans. on Mag. MAG-18,60, (1982)
- 3) J.D. Powell et al., IEEE Trans. on Mag.18, 7 (1982)
- 4) R. G. Mongeau et al., IEEE Trans on Mag. MAG-18, 7 (1982)
- 5) F. W. Grover, "Formulas for Mutual and Self Inductance", (Dover Publications, New York 1962)
- 6) H. B. Brooks, J. Res. Nat. Bur. Stand. 1, 289, (1951)
- 7) Campbell and Foster, "Tables of Fourier Integrals" (Van Nostrand & Co., New York) p. 166, formula 17

APPENDIX B

COMPUTER ALGORITHM FOR "SYNCHRONOUS COAXIAL ACCELERATOR"

The force equation and circuit equation for the ℓ^{th} coil are given respectively by

$$m \frac{dv}{dt} + \alpha v = I I_o \frac{\partial M}{\partial s} (x) \quad (B1)$$

and

$$L \frac{dI}{dt} + v I_o \frac{\partial M(x)}{\partial s} + R I = E(t) \quad (B2)$$

where all quantities are related to the ℓ^{th} coil. Using x as a variable we can write these equations as

$$\frac{d^2 x}{dt^2} + \frac{\alpha}{m} \frac{dx}{dt} = I \left(\frac{I_o}{m} \right) \frac{\partial M}{\partial s} (x) \quad (B3)$$

and

$$L \frac{dI}{dt} + I_o \frac{dx}{dt} \frac{\partial M}{\partial s} + R I = E(t) \quad (B4)$$

These equations can be reduced into coupled sets of linear equations by using the following substitutions.

<u>Old variable</u>	<u>New variable</u>	
t	x_1	
x	x_2	
x'	x_3	
I	x_4	(B5)

We then obtain the following set of linear differential equations

$$\begin{aligned}
x_1' &= 1 \\
x_2' &= x_3 \\
x_3' &= -\frac{\alpha}{m} x_3 + \frac{I_0}{m} \frac{\partial M}{\partial s}(x_2) x_4 \\
x_4' &= -\frac{I_0}{L} x_3 \frac{\partial M(x_2)}{\partial s} - \frac{R}{L} x_4 - \frac{E(x_1)}{L}
\end{aligned} \tag{B6}$$

This set can be written as

$$\bar{X}' = \bar{F}(\bar{X}) \tag{B7}$$

with the initial condition at $t = t_\ell$

$$\bar{X} = \begin{bmatrix} t_{\ell-1} \\ X_{\ell-1} \\ V_{\ell-1} \\ I_c \end{bmatrix} \quad \text{Note at } x_1 = 0 \quad \bar{X}_1 = \begin{bmatrix} 0 \\ 0 \\ 0 \\ I_c \end{bmatrix} \tag{B8}$$

These sets of equations can then be solved by using Runge-Kutta procedure.

In order to carry the solutions the following parameters should be specified:

1. $\frac{\partial M}{\partial s}(x)$, the rate of change of mutual inductance between the coils as a function of the distance x . $\frac{\partial M}{\partial s}(x)$ can be calculated for various coul configurations and its spatial dependence is substituted into the above equations. $\frac{\partial M}{\partial s}(x)$ for Brooks coil, as well as, other coils can be used in the equations.

2. The propagation voltage pulse $E(t)$ should also be specified. For simplicity, $E(t)$ can be taken as a step function propagating along the transmission line connecting the stationary coils.

3. Initial conditions: (fig. B2) set of linear differential equations given by equation B7 are written for the ℓ^{th} stationary coil when the projectile is interacting with this coil. This is an initial value problem for each of the initial

values for $x_1 = t$, $x_2 = x$, $x_3 = \frac{dx}{dt} = v$ and $x_4 = I$ should be specified. For the first coil ($\ell=1$) at $t=0$, $x=0$ and $V=0$ with $I=I_c$. The time it takes for the projectile to traverse the first coil, the distance and velocity at the end of this transversal become the initial conditions for the second coil. The current flowing in the projectile is assumed to have the same value I_c with the condition that I_c is switched to opposite polarity when $\frac{\partial M}{\partial s}(x)=0$ is reached, i.e. when the two coils have the maximum mutual inductance.

The initial condition for the ℓ^{th} coil is obtained from the final time, location and velocity of the projectile after the interaction between the projectile and $(\ell-1)^{\text{th}}$ coil is completed.

4. Friction between the brushes and the rail should be specified in the equation of motion for the projectile. α can be set equal to zero for no frictional case, α can be taken as constant for initial few coils or α can be written as a function of velocity to include the most general behavior of the interaction.

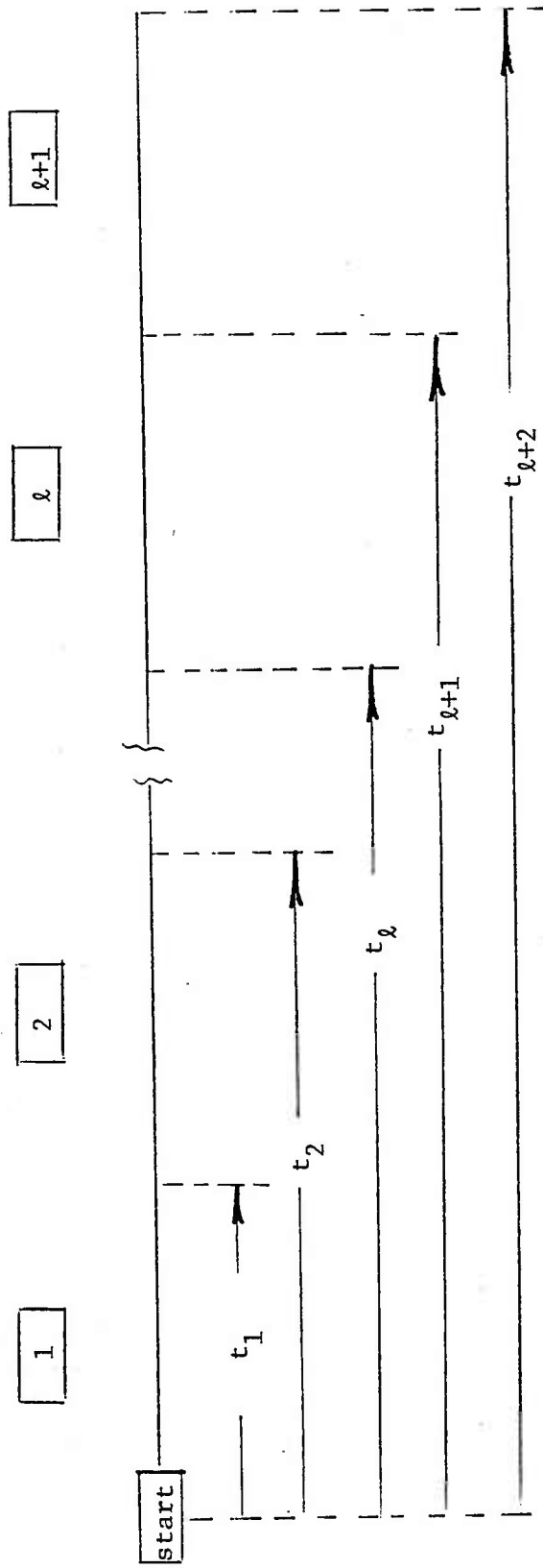


Figure B1. Initial conditions.

DISTRIBUTION LIST

Commander

Armament Research and Development Center
U.S. Army Armament, Munitions and Chemical Command
ATTN: DRSMC-TSS(D) (5)
DRSMC-GCL(D)
Dover, NJ 07801

Administrator

Defence Technical Information Center
ATTN: Accessions Division (12)
Cameron Station
Alexandria, VA 22314

Director

U.S. Army Material Systems Analysis Activity
ATTN: DRXSY-MP
Aberdeen Proving Ground, MD 21005

Commander

Chemical Research and Development Center
U.S. Army Armament, Munitions and Chemical Command
ATTN: DRSMC-CLJ-L(A)
DRSMC-CLB-PA(A)
APG, Edgewood Area, MD 21010

Director

Ballistics Research Laboratory
Armament Research and Development Center
U.S. Army Armament, Munitions and Chemical Command
ATTN: DRSMC-BLA-S(A)
Aberdeen Proving Ground, MD 21005

Chief

Benet Weapons Laboratory, LCWSL
Armament Research and Development Center
U.S. Army Armament, Munitions and Chemical Command
ATTN: DRSMC-LCB-TL

Commander

U.S. Army Armament, Munitions and Chemical Command
ATTN: DRSMC-LEP-L(R)
Rock Island, IL 61299

Director

U.S. Army TRADOC Systems
Analysis Activity
ATTN: ATAA-SL
White Sands Missile Range, NM 88002